

Lemaitre–Tolman–Bondi collapse from the perspective of loop quantum gravity

Martin Bojowald*

Institute for Gravitation and the Cosmos, The Pennsylvania State University,
104 Davey Lab, University Park, PA 16802, USA

Tomohiro Harada†

Department of Physics, Rikkyo University, Toshima, Tokyo 171-8501, Japan
and Rakesh Tibrewala‡

Tata Institute of Fundamental Research,
Homi Bhabha Road, Mumbai 400 005, India

Abstract

Lemaitre–Tolman–Bondi models as specific spherically symmetric solutions of general relativity simplify in their reduced form some of the mathematical ingredients of black hole or cosmological applications. The conditions imposed in addition to spherical symmetry turn out to take a simple form at the kinematical level of loop quantum gravity, which allows a discussion of their implications at the quantum level. Moreover, the spherically symmetric setting of inhomogeneity illustrates several non-trivial properties of lattice refinements of discrete quantum gravity. Nevertheless, the situation at the dynamical level is quite non-trivial and thus provides insights to the anomaly problem. At an effective level, consistent versions of the dynamics are presented which implement the conditions together with the dynamical constraints of gravity in an anomaly-free manner. These are then used for analytical as well as numerical investigations of the fate of classical singularities, including non-spacelike ones, as they generically develop in these models. None of the corrections used here resolve those singularities by regular effective geometries. However, there are numerical indications that the collapse ends in a tamer shell-crossing singularity prior to the formation of central singularities for mass functions giving a regular conserved mass density. Moreover, we find quantum gravitational obstructions to the existence of exactly homogeneous solutions within this class of models. This indicates that homogeneous models must be seen in a wider context of inhomogeneous solutions and their reduction in order to provide reliable dynamical conclusions.

*e-mail address: bojowald@gravity.psu.edu

†e-mail address: harada@rikkyo.ac.jp

‡e-mail address: rtibs@mailhost.tifr.res.in

1 Introduction

Black holes provide one of the most active areas of gravitational research, and a prime testing ground for quantum gravity. Many aspects can already be analyzed under the assumption of spherical symmetry, which is sufficient to describe non-rotating black holes. In vacuum, for instance, a reduced quantization is possible [1, 2, 3]. This reduction has thus often been used in diverse approaches to quantum gravity, and also loop quantum gravity [4, 5, 6] has provided its own formulation [7, 8, 9, 10, 11]. This allows one to use the loop representation constructed in the full theory in a simpler setting in which, as one hopes, one can find and analyze physical solutions. The result is a set of many coupled partial difference equations for a wave function on midisuperspace, which reflects the discreteness of spatial geometry realized in a loop quantization. As a consequence, spacelike classical singularities as they occur e.g. in the best-known case of the Schwarzschild solution are removed because their high curvature regimes no longer present boundaries to quantum evolution [12, 13]. So far, these present the only inhomogeneous singularities analyzed by the methods of loop quantum gravity, and the situation appears much more non-trivial than in homogeneous models. Due to this complexity, several questions remain open. In particular, inhomogeneous models allow not only spacelike singularities but also null or timelike ones, which may even be naked; see e.g. [14, 15, 16] and references therein. Their fate presents additional problems of high interest which can be studied in spherical symmetry.

Unfortunately, even the spherically symmetric equations in loop quantum gravity are difficult to tackle, and so it becomes interesting to look at further reductions which can preserve the physical setting but provide mathematical simplifications. Some of the possible effects have been introduced in a more ad-hoc manner in the models of [17, 18, 19, 20], and were used mainly to understand implications on the horizon dynamics. A drawback of such an approach is that quantum corrections are not clearly linked to key ingredients of a loop quantization, or any quantization one could apply to the full, unrestricted theory. We thus intend to introduce new models which, starting from the spherically symmetric reduction along the general lines of [8], provide further simplifications. Moreover, we will pay special attention to the anomaly problem which is required for full consistency. The possibility followed here is a reformulation of the spherically symmetric constrained system as it is used in the canonical definition of Lemaitre–Tolman–Bondi (LTB) models [21, 22, 23]. In this classical reduction, one solves the diffeomorphism constraint and, inserting the solutions into the Hamiltonian constraint, simplifies the set of equations. This eliminates some of the equations and removes several gauge issues. The remaining equations are then easier to quantize and solve.

The imposed conditions make the constrained system partially second class, and thus are not straightforward to implement at the quantum level. Symmetry reduction, which is also partially second class and can be done at the kinematical quantum level [7, 24, 25, 26, 27], provides some guidelines, but the gauge fixing conditions required for LTB models are more complicated. While these issues are discussed here, we postpone a direct implementation at the dynamical quantum level and rather perform in this article an analysis

of the quantum correction terms one can expect for the classical equations. Nevertheless, we will be able to highlight several important issues at the quantum level, such as the role of dynamical lattice refinements of discrete states [28, 29]. In particular, we will see that not all refinement schemes discussed so far in anisotropic homogeneous models can be embedded in spherically symmetric ones. But a large class still remains because only the direction dependence, not the size dependence of refinements is determined.

What we provide in the main part of this paper is an analysis of consistent sets of quantum corrected equations of motion for a type of non-perturbative inhomogeneities, which has not yet been available in other models studied in the framework of loop quantum gravity. Previous equations either refer to homogeneous models [30, 31, 32, 33], where strict effective equations can be derived as analyzed in a canonical setting in [34, 35, 36], but the consistency issue trivializes, or to perturbative inhomogeneities as in [37, 38, 39, 40, 41, 42, 43, 44]. In our case, inhomogeneities can be non-perturbative but their equations are arrived at only after performing a partial gauge fixing.

We will thus be able to restrict the form of possible quantum corrections by the condition that they provide consistent deformations of the classical equations. Thus, we will discuss how quantum corrections due to loop quantum gravity should occur in order to guarantee consistent LTB-like solutions. We will not be deriving strict effective equations, but we will determine consistent anomaly-free consequences of different types of quantum corrections. For several of the consistent choices we study consequences for inhomogeneous spherically symmetric systems based on analytical as well as numerical considerations. Our main interest here, as often in this context, is the fate of classical singularities. Compared to other models which by now have been studied extensively in loop quantum cosmology [45], a new feature is the possibility of non-spacelike singularities in LTB systems. Interestingly, none of the corrections studied here resolve such singularities directly (nor spacelike ones in these models), in contrast to what their analogs do so easily in homogeneous models. However, numerically we find indications that shell-crossing singularities generically occur in the presence of the corrections, where only shell-focusing singularities would do in classical theory. The shell-crossing singularities are expected to be weakly extendable, or to be avoidable by realistic matter. This is one example for new effects in inhomogeneous models, which not surprisingly prove themselves much more non-trivial than homogeneous ones.

2 Spherically symmetric spacetimes and LTB variables

The line element in a general spherically symmetric spacetime with polar coordinates (x, ϑ, φ) can be written as

$$ds^2 = -e^{2\nu} dt^2 + e^{2\lambda} dx^2 + R^2(d\vartheta^2 + \sin^2 \vartheta d\varphi^2), \quad (1)$$

where $\nu = \nu(t, x)$, $\lambda = \lambda(t, x)$ and $R = R(t, x)$ are functions of the time and radial coordinates t and x . Alternatively, the form suitable for a canonical analysis, as done

below, is

$$ds^2 = -N(x, t)^2 dt^2 + L(x, t)^2 (dx + N^x(x, t) dt)^2 + R(x, t)^2 (d\vartheta^2 + \sin^2 \vartheta d\varphi^2) \quad (2)$$

where N , N^x , L and R are again free functions of the radial coordinate x and time t only. In a canonical quantization, the lapse function N and the shift vector N^x appear as Lagrange multipliers of the Hamiltonian and diffeomorphism constraints, respectively. They are thus not dynamical, unlike the remaining functions L and R which have non-trivial momenta P_L and P_R , together forming the kinematical phase space of spherically symmetric gravity. In (1), the shift vector has already been chosen to vanish, while ν and λ are related to N and L in obvious ways.

2.1 Matter source

We start with a spherically symmetric matter source whose stress-energy tensor T_ν^μ is diagonalized in the form

$$T_\nu^\mu = \begin{pmatrix} -\epsilon & 0 & 0 & 0 \\ 0 & \Sigma & 0 & 0 \\ 0 & 0 & \Pi & 0 \\ 0 & 0 & 0 & \Pi \end{pmatrix}, \quad (3)$$

where $\epsilon = \epsilon(t, x)$, $\Sigma = \Sigma(t, x)$ and $\Pi = \Pi(t, x)$ are the energy density, the radial pressure and the tangential pressure, respectively. Einstein's equation and the conservation law then reduce to a set of partial differential equations given by

$$m' = 4\pi G \epsilon R^2 R' \quad (4)$$

$$\dot{m} = -4\pi G \Sigma R^2 \dot{R} \quad (5)$$

$$\dot{R}' = \dot{R} \nu' + R' \dot{\lambda} \quad (6)$$

$$\Sigma' = -(\epsilon + \Sigma) \nu' - 2(\Sigma - \Pi) \frac{R'}{R} \quad (7)$$

$$e^{-2\nu} (\ddot{R} - \dot{\nu} \dot{R}) - e^{-2\lambda} \nu' R' = -\frac{m}{R^2} - \frac{4}{3} \pi (\Sigma + 2\Pi) R \quad (8)$$

where we have introduced

$$m = \frac{R}{2} \left(1 - R'^2 e^{-2\lambda} + \dot{R}^2 e^{-2\nu} \right), \quad (9)$$

called the Misner–Sharp mass.

The Misner–Sharp mass m is generally defined as

$$m = \frac{1}{2} R (1 - \nabla_A R \nabla^A R), \quad (10)$$

where A takes values 0 and 1 corresponding to the 2-manifold coordinatized by t and x . At spherical trapping horizons [46] we have $R = 2m$. (To see this, one can use the simple

criterion for the spherically symmetric trapping horizon as the place where constant area radius surfaces become null [47]. This is the boundary of the region of spherical trapped surfaces; there may be non-spherical trapped surfaces outside that region [48, 49].) In an asymptotically flat spacetime, the asymptotic value of the Misner–Sharp mass at spatial infinity equals the ADM mass M_{ADM} . We can define a conserved current from the Misner–Sharp mass, which is called the Kodama current and given by

$$j^A = \epsilon^{AB} \nabla_B m, \quad (11)$$

where ϵ_{AB} is the antisymmetric tensor satisfying $\epsilon_{AB}\epsilon^B{}_C = g_{AC}$. By definition, the current j^A satisfies the conservation law $\nabla_A j^A = 0$. The Kodama current provides the energy density

$$\epsilon = \frac{m'}{4\pi G R^2 R'} \quad (12)$$

in agreement with (4).

2.2 Classical LTB spacetimes

In classical Einstein gravity, there is an exact solution which describes a spherically symmetric collapse system sourced by inhomogeneous dust: the Lemaitre–Tolman–Bondi solution [21, 22, 23]. For dust, we have $\Sigma = \Pi = 0$ such that Eq. (5) implies that

$$m = \frac{1}{2} F(x) \quad (13)$$

is an arbitrary function of the radial coordinate only. From Eq. (4), we then have

$$\epsilon = \frac{F'}{8\pi G R^2 R'} \quad (14)$$

for the dust density. Then, Eq. (7) implies that $\nu = \nu(t)$ can be made to vanish by rescaling the time coordinate t such that it becomes the dust proper time. Eq. (6) can be integrated to give

$$(R' e^{-\lambda})^2 = 1 + \kappa(x), \quad (15)$$

where $\kappa(x) > -1$ is another arbitrary function. The resulting line element can be written as

$$ds^2 = -dt^2 + \frac{R^2}{1 + \kappa(x)} dx^2 + R^2 (d\vartheta^2 + \sin^2 \vartheta d\varphi^2) \quad (16)$$

where the only dynamical function left satisfies, from Eq. (9),

$$\dot{R}^2 = \kappa(x) + \frac{F(x)}{R}. \quad (17)$$

Here we concentrate on the special case where $\kappa(x) = 0$, called marginally bound LTB solution, such that

$$ds^2 = -dt^2 + R'^2 dx^2 + R^2 (d\vartheta^2 + \sin^2 \vartheta d\varphi^2) \quad (18)$$

and Eq. (17) becomes

$$\dot{R}^2 = \frac{F(x)}{R}. \quad (19)$$

At a trapping horizon, this expression equals one. We can integrate the equation of motion to

$$t - t_s(x) = \pm \frac{2R^{3/2}}{3F(x)^{1/2}}, \quad (20)$$

where $t_s(x)$ is an arbitrary function specifying initial values at $t = 0$. Its freedom can be absorbed by defining the function R in terms of the coordinate x at $t = 0$. For instance, requiring $R|_{t=0} = x$ and choosing the lower sign in (20) for a collapsing model, we have $t_s(x) = \frac{2}{3}x^{3/2}F(x)^{-1/2}$ and thus

$$R(x, t) = \left(x^{3/2} - \frac{3}{2}\sqrt{F(x)t} \right)^{2/3}. \quad (21)$$

(An example is the self-similar solution $R = x(1 - at/x)^{2/3}$ obtained for $F(x) = \lambda x$ as studied in [50].) Of special interest in those solutions is the small- x behavior of R which may be regular or singular. In particular, the energy density (14) can be divergent where $R' = 0$, giving rise to shell-crossing singularities. While solutions are no longer valid beyond this point, shell-crossing singularities are deemed avoidable by more realistic matter models; see e.g. [51]. Moreover, solutions are extendable through shell-crossing singularities in a distributional sense [52, 53]. In addition to this, energy density as well as the Ricci scalar can diverge when $R = 0$, giving rise to a shell-focusing or central singularity which is the main interest here. The properties of shell-focusing singularities in LTB models have been extensively studied [54, 55, 56, 57]. In particular, it was proven that naked singularities form generically in this system [55, 58, 59].

This provides a new arena for effects of quantum gravity, which we will come back to in more detail in Sec. 5. We will be using loop quantum gravity which requires Hamiltonian techniques. In the canonical formulation of spherically symmetric Einstein gravity, the Hamiltonians of the gravitational sector, H_{grav} , and of the matter sector, H_{dust} , for the LTB system provide the expressions

$$H_{\text{grav}} = -\frac{\dot{R}^2 R' + R(\dot{R}^2)'}{2G} = -\frac{(\dot{R}^2 R)'}{2G}, \quad H_{\text{dust}} = \frac{F'}{2G} \quad (22)$$

after replacing the momentum in terms of \dot{R} . The total Hamiltonian constraint $H_{\text{grav}} + H_{\text{dust}} = 0$ then yields Eq. (19). Below, we will provide a detailed canonical analysis based on Ashtekar variables, which will allow us to incorporate some corrections as they are expected from loop quantum gravity. (See [60, 61, 62] for a canonical analysis in ADM variables, and [63, 64] for an analysis in arbitrary dimensions.)

2.3 Connection variables

For a canonical formulation only the spatial part of the metric provides the dynamical degrees of freedom. Moreover, the most successful canonical quantization of gravity, loop

quantum gravity, is based on a densitized triad E_i^a rather than a spatial metric q_{ab} , which are related by $E_i^a E_i^b = \det(q_{cd}) q^{ab}$. (We use tangent space indices a, b, \dots and internal gauge indices i, j, \dots) The spatial metric for a spherically symmetric system in components of this variable is given by

$$ds^2 = \frac{E^\varphi(x)^2}{|E^x(x)|} dx^2 + |E^x(x)| (d\vartheta^2 + \sin^2 \vartheta d\varphi^2) \quad (23)$$

where instead of the spherically symmetric spatial metric components L (which equals $E^\varphi/\sqrt{|E^x|}$) and R (which equals $\sqrt{|E^x|}$) the spherically symmetric triad components E^x and E^φ appear. Written as a densitized vector field taking values in $\mathfrak{su}(2)$ with basis τ_i , these components define the spherically symmetric densitized triad by

$$E = E^x(x)\tau_3 \sin \vartheta \frac{\partial}{\partial x} + (E^1(x)\tau_1 + E^2(x)\tau_2) \sin \vartheta \frac{\partial}{\partial \vartheta} + (E^1(x)\tau_2 - E^2(x)\tau_1) \frac{\partial}{\partial \varphi}. \quad (24)$$

such that $(E^\varphi)^2 = (E^1)^2 + (E^2)^2$. (For more details on this decomposition see [7, 8]. Notice that the sign of E^x is not restricted to be positive, while E^φ is defined to be non-negative. The sign of E^x thus determines the orientation of the triad since $\text{sgn} \det(E_i^a) = \text{sgn} E^x$; it plays an important role for fundamental singularity resolution [13], but not for most of the analysis done in this article.) The remaining freedom of the three functions E^x , E^1 and E^2 not contained in the components E^x and E^φ is pure gauge since it does not affect the metric. It can be parameterized by an angle $\eta = \arctan(E^2/E^1)$ which is subject to $U(1)$ -gauge transformations. The corresponding Gauss constraint is $G[\lambda] = \int dx \lambda(x) ((E^x)' + P^\eta)$ where P^η is the momentum of η .

Fields canonically conjugate to the original triad components E^I are Ashtekar connection components of

$$A = A_x(x)\tau_3 dx + (A_1(x)\tau_1 + A_2(x)\tau_2) d\vartheta + (A_1(x)\tau_2 - A_2(x)\tau_1) \sin \vartheta d\varphi + \tau_3 \cos \vartheta d\varphi. \quad (25)$$

Also here we introduce the $U(1)$ -gauge invariant quantity $A_\varphi^2 = A_1^2 + A_2^2$ and the gauge angle $\beta = \arctan(A_2/A_1)$. Only the difference $\alpha := \eta - \beta$ of the angles is gauge invariant, while each of them can be changed by the same amount with a gauge transformation. However, the new parameter A_φ is not canonically conjugate to E^φ ; see [8] for details. In terms of the $U(1)$ -gauge invariant triad component E^φ , its conjugate variable is rather given by $A_\varphi \cos \alpha = \gamma K_\varphi$ which happens to be proportional to an extrinsic curvature component [9]. (The constant of proportionality is given by the Barbero–Immirzi parameter γ [65, 66].) The canonical pairs we will be dealing with are thus (A_x, E^x) , $(\gamma K_\varphi, E^\varphi)$ for which

$$\{A_x(x), E^x(y)\} = 2\gamma G \delta(x, y) \quad , \quad \{\gamma K_\varphi(x), E^\varphi(y)\} = \gamma G \delta(x, y) \quad (26)$$

and another pair (η, P^η) for the gauge angle. The relation between the remaining Ashtekar connection component A_x and extrinsic curvature is $A_x = \gamma K_x - \eta'$ where the spatial derivative η' of the angle is the (negative) x -component of the spin connection. Its angular components are given in terms of

$$\Gamma_\varphi = -\frac{(E^x)'}{2E^\varphi} \quad (27)$$

which determines the relation between A_φ and K_φ as $A_\varphi^2 = \Gamma_\varphi^2 + \gamma^2 K_\varphi^2$ without reference to α .

Solving the Gauss constraint removes the gauge angle and its momentum, and implies that invariant objects can depend on the x -component of the Ashtekar connection only through the extrinsic curvature quantity $A_x + \eta' = \gamma K_x$. We are then left with only two canonical pairs (K_x, E^x) and (K_φ, E^φ) . A further reduction can be implemented by using the LTB form of the variables corresponding to the metric (18). Comparing the spatial parts of the metrics (18) and (23) one obtains the LTB relation

$$E^\varphi(x) = \frac{1}{2}|E^x(x)|'. \quad (28)$$

In particular, we have $\Gamma_\varphi = -\text{sgn}E^x$ everywhere. For a complete reduction of canonical degrees of freedom, this is to be accompanied by a condition between K_x and K_φ . We will determine this by consistency with the constraints, such that (28) is preserved in time.

2.4 Constraints

Constraints in real Ashtekar variables as used here have been derived in [8, 9]. The diffeomorphism constraint is given by

$$D[N^x] = \int dx N^x (2A_1' E^1 + 2A_2' E^2 - A_x (E^x)') \quad (29)$$

where $A_1 = A_\varphi \sin \beta$, $A_2 = -A_\varphi \cos \beta$, $E^1 = E^\varphi \sin \eta$, $E^2 = -E^\varphi \cos \eta$. Using these definitions in the above equation one obtains

$$D[N^x] = \int dx N^x (2(A_\varphi \cos \alpha)' E^\varphi + 2(\alpha' + \beta') E^\varphi A_\varphi \sin \alpha - A_x (E^x)') \quad (30)$$

Using the relations $A_\varphi \cos \alpha = \gamma K_\varphi$, $A_\varphi \sin \alpha = \Gamma_\varphi$, $\alpha + \beta = \eta$, $A_x = -\eta' + \gamma K_x$ and $\Gamma_\varphi = -(E^x)' / 2E^\varphi$, this can be expressed solely in terms of U(1)-gauge invariant quantities as

$$D[N^x] = \int dx N^x (2\gamma K_\varphi' E^\varphi - \gamma K_x (E^x)') . \quad (31)$$

We can consider the marginally bound LTB condition, as given by (28), as a gauge-fixing condition of the diffeomorphism constraint to form a second class pair. On the gauge fixing surface, the diffeomorphism constraint can be replaced by

$$D[N^x] = \int dx N^x \gamma (E^x)' (\text{sgn}(E^x) K_\varphi' - K_x) . \quad (32)$$

Thus, for the diffeomorphism constraint to be satisfied one must have

$$K_\varphi' = K_x \text{sgn} E^x . \quad (33)$$

This provides the LTB condition for the conjugate variables to E^I analogous to (28). Having solved the second class constraints resulting from gauge-fixing $D[N^x]$, we proceed to the Hamiltonian constraint and insert the solutions.

In spherical symmetry, the gravitational part of the Hamiltonian constraint is

$$H_{\text{grav}}[N] = -\frac{1}{2G} \int dx N(x) |E^x|^{-1/2} \left((1 - \Gamma_\varphi^2 + K_\varphi^2) E^\varphi + 2\gamma^{-1} K_\varphi E^x (A_x + \eta') + 2E^x \Gamma'_\varphi \right). \quad (34)$$

With $\Gamma_\varphi = -1$ under the LTB condition in (28), we have

$$H_{\text{grav}}[N] = -\frac{1}{2G} \int dx N(x) |E^x|^{-1/2} \left(K_\varphi^2 E^\varphi + 2K_\varphi E^x K_x \right) \quad (35)$$

or, in unsmeared form,

$$H_{\text{grav}} = -\frac{1}{2G} \left(\frac{K_\varphi^2 E^\varphi}{\sqrt{|E^x|}} + 2K_\varphi K_x \sqrt{|E^x|} \right) \quad (36)$$

where E^φ and K_φ are to be understood as functionals of E^x and K_x , respectively, via the LTB conditions, or as functions of R and its momentum P_R . Thus, H_{grav} is left as the sole constraint to restrict initial values and generate equations of motion for LTB models. In fact, the conditions (28) and (33) can be seen to be consistent with the classical equations of motion for E^x , E^φ , K_x and K_φ generated by (36) (in addition to solving the diffeomorphism constraint identically). Thus, the reduction to LTB form is dynamically consistent and provides correct space-time solutions. Maintaining this consistency will be our main guideline in the analysis of quantum effects.

3 Effects of a loop quantization

Like any quantization of an interacting system, quantum gravity implies corrections to classical equations of motion and thus forces us to re-address consistency issues of classical reductions. As we will see explicitly, for a loop quantization this provides valuable feedback on the consistency or possible anomalies of the overall framework. In LTB systems, once a consistent reduction has been found, it can be used for applications to black hole singularity issues. We focus on loop specific issues which do not arise in Wheeler–DeWitt type quantizations of [60, 61, 62] which have for instance been applied to Hawking radiation [67, 68, 64].

3.1 Basics of spherically symmetric loop quantum gravity

A loop quantization [69] of spherically symmetric gravity is based on holonomies

$$h_e(A_x) = \exp\left(\frac{1}{2}i \int_e A_x dx\right) \quad , \quad h_v(K_\varphi) = \exp(i\gamma K_\varphi(v)) \quad , \quad h_v(\eta) = \exp(i\eta(v)) \quad (37)$$

for the configuration variables instead of linear expressions in connection or extrinsic curvature components. Here, we have used edges e and vertices v in the radial line. The use of these variables is strongly motivated by general results of loop quantum gravity [4, 5, 6]: Background independence, i.e. quantization in the absence of a metric other than the physical one determined by E_i^a , is realized in a well-defined representation of smeared basic variables for holonomies together with fluxes as 2-dimensionally integrated densitized triads. But operators for connection or extrinsic curvature components themselves do not exist.

An orthonormal basis of gauge invariant states in the connection representation is given by [8]

$$T_{g,k,\mu} = \prod_{e \in g} \exp\left(\frac{1}{2} i k_e \int_e (A_x + \eta') dx\right) \prod_{v \in g} \exp(i \mu_v \gamma K_\varphi(v)) \quad (38)$$

with integer labels k_e and positive real labels μ_v on edges e and vertices v , respectively, forming a finite graph g in the 1-dimensional radial line. The labels determine the connection dependence by irreducible representations of the groups spanned by the holonomies. (These groups are $U(1)$ for A_x -holonomies and the Bohr compactification $\overline{\mathbb{R}}_{\text{Bohr}}$ of the real line for K_φ -holonomies; see [8] for details.) The densitized triad, i.e. momenta conjugate to the connection components, will be derivative operators which are quantized in the full theory in the form of fluxes $\int_S E_i^a \tau^i n_a d^2 y$ as integrals over surfaces S with co-normals n_a . Their explicit action in spherical symmetry is

$$\hat{E}^x(x) T_{g,k,\mu} = \gamma \ell_{\text{P}}^2 \frac{k_{e^+(x)} + k_{e^-(x)}}{2} T_{g,k,\mu} \quad (39)$$

$$\int_{\mathcal{I}} \hat{E}^\varphi T_{g,k,\mu} = \gamma \ell_{\text{P}}^2 \sum_{v \in \mathcal{I}} \mu_v T_{g,k,\mu} \quad (40)$$

where $\ell_{\text{P}}^2 = G\hbar$ is the Planck length squared and $e^\pm(x)$ denote the neighboring edges to a point x , distinguished from each other using a given orientation of the radial line. (We have $k_{e^+(x)} = k_{e^-(x)}$ if x is not a vertex of the graph.) The \hat{E}^φ -operators only exist in smeared form after integrating over arbitrary radial intervals \mathcal{I} . All flux operators have discrete spectra: eigenstates as seen in (39) and (40) are normalizable. But only \hat{E}^x has a discrete set of eigenvalues, while \hat{E}^φ -eigenvalues fill the real line. (Their eigenstates are elements of the non-separable Hilbert space of square integrable functions on the Bohr compactification of the real line.)

These basic operators can be used for composite operators as well, providing well-defined but rather complicated constraint operators. Instead of dealing directly with these operators, we will extract some typical effects as phenomenological corrections to the classical equations and analyze their potential implications with more ease. This has been done in quite some detail in cosmological applications [70, 39, 40, 41, 37, 42, 43, 44, 71, 72, 73], and we start the same in this paper for inhomogeneous models in the spherically symmetric context. In this way, we provide the first examples where full inhomogeneities, rather than perturbative ones as in cosmology, are studied in this way. But we emphasize that

we do not derive complete effective equations as per [34, 35, 36] in this paper, which is rather an exploration of possible effects. Nevertheless, restrictions by consistency already provide interesting lessons. The general consistency issue is similar to that studied after partial gauge fixings in spherical symmetry in [11], where it was analyzed based on the general ideas of [74, 75], and in [76]. Our analysis here provides complementary results in a different setting, where we make sure that potential anomalies arising from different correction terms cancel each other. Moreover, the effective treatment allows us to arrive more directly at properties of physical solutions.

3.2 Implementing the LTB conditions

The LTB conditions (28) and (33) in terms of densitized triad and extrinsic curvature variables are well-suited to an implementation at the level of spin networks. They refer directly to basic expressions of the quantization (provided that one just exponentiates the relation (33) to result in holonomies) and can thus easily be formulated as conditions for kinematical states. In this way, the LTB reduction can be performed at the quantum level. However, consistency issues of the dynamics are not easy to deal with at the complete quantum level. We will therefore describe the kinematical constructions here, proceed to a phenomenological effective level in Sec. 4 and then study its consistency. By the link to the initial loop quantization, this indirect route will nevertheless provide feedback on the full theory.

From the triad relation (28) we derive a condition for fluxes simply by integrating over arbitrary radial intervals \mathcal{I} :

$$\int_{\mathcal{I}} E^\varphi = \frac{1}{2} |E^x|_{\partial\mathcal{I}} \quad (41)$$

where $\partial\mathcal{I}$ is the boundary of \mathcal{I} at which E^x is evaluated, taking into account orientation to have the correct signs. This relation can be imposed on triad eigenstates (38), where (39) and (40) imply

$$\mu_v = \frac{1}{2} (|k_{e^+(v)}| - |k_{e^-(v)}|) \quad (42)$$

for any vertex v . This directly eliminates all vertex labels in favor of the edge labels which remain free, analogously to the function $|E^x| = R^2$ which classically determines an LTB metric completely.

On these reduced states, it turns out, the LTB condition for holonomy operators is already implemented. Upon integration and exponentiation, we have

$$\exp\left(\frac{1}{2} i \text{sgn}(E^x) \int_{v_1}^{v_2} (A_x + \eta') dx\right) = \exp\left(\frac{1}{2} i \gamma K_\varphi(v_1)\right) \exp\left(-\frac{1}{2} i \gamma K_\varphi(v_2)\right) \quad (43)$$

expressed solely in terms of elementary holonomy operators. This condition is realized in the sense that the left and right hand sides, as multiplication operators, have the same action on solutions to the LTB condition satisfying (42). In fact, the left hand side simply increases the label of the edge between v_1 and v_2 (which we assume to be two adjacent

vertices) by one. Thus, it changes both $k_{e+(v_1)}$ and $k_{e-(v_2)}$ by ± 1 depending on their sign. The two operators on the right hand side, on the other hand, change the vertex label μ_{v_1} by $\frac{1}{2}$ and μ_{v_2} by $-\frac{1}{2}$ in the right way to respect the condition (42) if it was realized for the original state. (If there are vertices v between v_1 and v_2 , $k_{e+(v)}$ and $k_{e-(v)}$ change by the same value such that (42) remains implemented without changing μ_v .)

Notice that, unlike conditions for a symmetry reduction, the two LTB conditions for densitized triads and extrinsic curvature have vanishing Poisson brackets with each other (but not with the constraints). Thus, the curvature condition can indeed be implemented on the solution space of the triad condition. It does not add further conditions for states because they are written in a specific polarization. LTB states are thus simply represented by a chain of integer labels k_n for $n = 0, 1, \dots$ which represents spatial discreteness (a 1-dimensional lattice of independent sites) as well as the discreteness of quantum geometry (integer k_n as eigenvalues of the area radius squared). In a connection representation, they can be written as $T_k^-(z_0, z_1, \dots) = \prod_n z_n^{k_n}$ where the assignment $n \mapsto z_n := \exp(\frac{1}{2}i \int_{e_n} \gamma K_x dx)$ is a generalized LTB connection.

While states can be reduced immediately to implement the LTB conditions, further conditions do result for composite operators because (43) must be used if the action of any operator is to be written on the LTB states where (42) has eliminated vertex labels. This provides reductions, e.g. of constraint operators, such that characteristic quantum gravity effects in loop operators can be carried over to constraints for an LTB model.

3.3 Inverse triad effects

The first effect we turn to arises from the required quantization of inverse powers of the densitized triad, such as E^x in (36). There is no direct quantization of such an inverse since \hat{E}^x in a loop quantization (39) has a discrete spectrum containing zero, and thus lacks an inverse operator. Nevertheless, one can use general techniques to arrive at a well-defined operator which reproduces $(E^x)^{-1}$ in a classical limit. This quantization is based on the Poisson relation between a holonomy and the volume, which one can identify with an expression for $\frac{1}{\sqrt{|E^x|}}$. More precisely, we have $4\pi\gamma G \text{sgn}(E^x) E^\varphi / \sqrt{|E^x|} = \{A_x, V\}$ for the combination of triad components appearing in the first term of (36), where $V = 4\pi \int dx \sqrt{|E^x|} E^\varphi$ is the classical expression for volume in spherically symmetric setting. In these expressions, we follow general constructions of the full theory [77].

When quantized, the connection component is expressed through a holonomy, and the Poisson bracket becomes a commutator. In order to stay as close to the full theory as possible, we use SU(2)-holonomies

$$h_x(A) = \exp(\tau_3 \int A_x) = \cos(\frac{1}{2} \int A_x) + 2\tau_3 \sin(\frac{1}{2} \int A_x) \quad (44)$$

which in their matrix elements provide the basic quantities (37). (Generators of SU(2) are $\tau_j = -\frac{1}{2}i\sigma_j$ in terms of Pauli matrices σ_j ; path ordering is not necessary for radial holonomies thanks to the symmetry reduction, which reduces the gauge group to an Abelian

one [7].) The commutator for these holonomies becomes

$$\begin{aligned} h_x[h_x^{-1}, \hat{V}] &= \hat{V} - \cos(\tfrac{1}{2} \int A_x) \hat{V} \cos(\tfrac{1}{2} \int A_x) - \sin(\tfrac{1}{2} \int A_x) \hat{V} \sin(\tfrac{1}{2} \int A_x) \\ &\quad + 2\tau_3 \left(\cos(\tfrac{1}{2} \int A_x) \hat{V} \sin(\tfrac{1}{2} \int A_x) - \sin(\tfrac{1}{2} \int A_x) \hat{V} \cos(\tfrac{1}{2} \int A_x) \right) \end{aligned} \quad (45)$$

and appears in the constraint in the form $\text{tr}(\tau_3 h_x[h_x^{-1}, \hat{V}])$. This can be used in a quantization of

$$\text{tr}(\tau_3 h_x\{h_x^{-1}, V\}) = -\text{tr}(\tau_3^2 \{ \int A_x, V \}) = \frac{1}{2} \int_e \{A_x, V\} \sim \frac{1}{2} \ell_0 \{A_x, V\}$$

where ℓ_0 is the coordinate length of the edge used. When inserted in the Hamiltonian constraint, ℓ_0 for all edges discretizes the integration measure dx . Eigenvalues can be computed easily from the basic action of holonomies and fluxes: for the operator

$$\begin{aligned} \int_{\mathcal{I}} \frac{\widehat{E^\varphi \text{sgn}(E^x)}}{\sqrt{|E^x|}} &= \frac{-i}{2\pi\gamma G\hbar} \text{tr}(\tau_3 h_x[h_x^{-1}, \hat{V}]) \\ &= \frac{-i}{2\pi\gamma G\hbar} \left(\sin(\tfrac{1}{2} \int A_x) \hat{V} \cos(\tfrac{1}{2} \int A_x) - \cos(\tfrac{1}{2} \int A_x) \hat{V} \sin(\tfrac{1}{2} \int A_x) \right) \end{aligned} \quad (46)$$

we have eigenvalues

$$\left(\int_{\mathcal{I}} \frac{\widehat{E^\varphi \text{sgn}(E^x)}}{\sqrt{|E^x|}} \right)_{k,\mu} = 2\sqrt{\gamma}\ell_P |\mu_v| \left(\sqrt{|k_{e^+(v)} + k_{e^-(v)} + 1|} - \sqrt{|k_{e^+(v)} + k_{e^-(v)} - 1|} \right) \quad (47)$$

where v is the starting point of the interval \mathcal{I} used as the edge in the holonomy.

Looked at for all values of E^x , eigenvalues of the resulting operator do not agree exactly with the classical function $E^\varphi/\sqrt{|E^x|}$ but show deviations especially at small E^x . We can parameterize this by a correction function $\alpha(E^x)$ as

$$\alpha(E^x) := \left(\frac{\widehat{1}}{\sqrt{|E^x|}} \right)_{k(E^x)} \left(\sqrt{|\hat{E}^x|} \right)_{k(E^x)} = 2 \frac{\sqrt{|E^x + \gamma\ell_P^2/2|} - \sqrt{|E^x - \gamma\ell_P^2/2|}}{\gamma\ell_P^2} \sqrt{|E^x|} \quad (48)$$

where the subscript $k(E^x)$ means that the eigenvalue of the operator is taken at label $k_{e^+(v)} + k_{e^-(v)} = 2E^x/\gamma\ell_P^2$ as it follows from (39). Classically, i.e. for $\ell_P \rightarrow 0$, we have $\alpha(E^x) = 1$, and this limit is approached by α for large E^x . With the correction, the expression for the inverse power of the triad component E^x is finite, just as in the isotropic case [78]. The general behavior of the correction function is illustrated in Fig. 1 below. Similar constructions have been used before in spherical symmetry, see e.g. [17]. (While finiteness of inverse triad operators is realized in isotropic and spherically symmetric models, this is not expected to be a general property [79, 80]. Nevertheless, inverse triad operators are well-defined in general situations of loop quantum gravity [81].)

One should note that E^x refers to the total area of a whole orbit at radius x , which can have macroscopic values. In this case, α only slightly differs from one. However, a fully inhomogeneous quantization would refer to flux values of individual microscopic patches, where $E^x = \sum_n p_n$ is a large sum of microscopic contributions p_n , together giving the whole orbit area. The single fluxes p_n are much smaller and closer to the Planck scale, which makes α differ from one more noticeably if these fundamental fluxes are used. This is an illustration of the fact that symmetric models often artificially suppress corrections from inverse triad operators, as first noted in [82]. Inverse triad corrections analogous to α have thus occasionally been underestimated, especially in isotropic models of macroscopic universes with large matter content. One can model the enhancements of corrections in fully inhomogeneous states even in symmetric models by using higher $SU(2)$ -representations of holonomies in operators, not just the fundamental one as understood in (46). Then, the expression for α changes essentially by replacing $\gamma\ell_P^2$ in (48) by $j\gamma\ell_P^2$ if j is the spin of the representation. (See [83, 84] for precise formulas in those cases.) For our qualitative analysis here we can focus on the expression (48). In fact, later applications mainly use the small- E^x behavior near a center or a central singularity where corrections are strong for any j .

Because classically, for $\ell_P \rightarrow 0$, the function $\alpha(E^x)$ approaches one, the classical limit is correct if this function is inserted as a multiplier of $1/\sqrt{E^x}$ in the Hamiltonian constraint. We can thus write (36) as

$$\begin{aligned} H_{\text{grav}}^{(I)} &= -\frac{1}{G} \left(\frac{\sqrt{|E^x + \gamma\ell_P^2/2|} - \sqrt{|E^x - \gamma\ell_P^2/2|}}{\gamma\ell_P^2} K_\varphi^2 E^\varphi + K_\varphi K_x \sqrt{|E^x|} \right) \\ &= -\frac{1}{2G} \left(\frac{\alpha(E^x)}{\sqrt{|E^x|}} K_\varphi^2 E^\varphi + 2K_\varphi K_x \sqrt{|E^x|} \right). \end{aligned} \quad (49)$$

The form of corrections is usually not fully unique due to the presence of quantization ambiguities. Sometimes, however, they can be restricted more strongly by relating, whenever possible, reduced expressions to what one expects in the full theory. This provides different options for specific corrections which can be analyzed for robustness and the phenomenology they imply. In the present case, the full theory may suggest an alternative corrected Hamiltonian

$$H_{\text{grav}}^{(II)} = -\frac{1}{2G} \frac{\alpha(E^x)}{\sqrt{|E^x|}} (K_\varphi^2 E^\varphi + 2K_\varphi K_x E^x). \quad (50)$$

Here, also the second term carries a correction function, which is motivated if one takes into account that the $\sqrt{|E^x|}$ in the second term of (36) arises from a cancellation in $E^x/\sqrt{|E^x|}$ after inserting spherically symmetric variables into the full constraint. Thus, the second term could also be expected to have a correction by α . We will analyze both cases below and describe the differences they imply.

3.4 Holonomy effects and lattice refinements

Another characteristic, and in fact eponymous, feature of loop quantum gravity is that not components of the connection but rather its holonomies are represented as operators. Since these are non-linear objects, additional corrections by higher order terms of the connection (or extrinsic curvature) will be present which again can be evaluated by including them as correction terms in phenomenological equations. This may appear as higher curvature corrections as they involve higher powers of extrinsic curvature, but we emphasize that this procedure will not give a complete picture since higher derivative terms are missing. These can be computed at an effective level [34, 35, 36], which would require much more work not pursued here.

We can correct for the holonomy effects in the Hamiltonian constraint (36) as follows. We assume K_x to be fairly constant over a given edge (or part of an edge for graph-changing operators) of the graph whose holonomies appear as basic loop variables, so that $\int_{v_-}^{v_+} K_x \approx \ell_0 K_x$ where ℓ_0 is the coordinate length of the edge lying between the vertices v_- and v_+ . Rather than using a precise loop quantization of (36) and computing its expectation value in terms of holonomies, we make the following replacements in the Hamiltonian constraint: $K_\varphi \rightarrow (\gamma\delta)^{-1} \sin(\gamma\delta K_\varphi)$ and $K_x \rightarrow (\gamma\ell_0)^{-1} \sin(\gamma K_x \ell_0)$. In addition to ℓ_0 , δ is a dimensionless parameter whose role is discussed below. With these corrections, the constraint becomes

$$H_{\text{grav}}^{(III)} = -\frac{1}{2G} \left(\frac{\sin^2(\gamma\delta K_\varphi)}{\gamma^2 \delta^2} \frac{E^\varphi}{\sqrt{|E^x|}} + 2 \frac{\sin(\gamma\delta K_\varphi)}{\gamma\delta} \frac{\sin(\gamma K_x \ell_0)}{\gamma\ell_0} \sqrt{|E^x|} \right). \quad (51)$$

While this may not be the precise result from a complete effective constraint, it captures the main effects of using holonomies as periodic, rather than linear, functions in the curvature components. Moreover, this simplest choice guarantees that also here the classical limit, which involves a continuum limit $\delta \rightarrow 0$ and $\ell_0 \rightarrow 0$, is satisfied. Note, however, that one should not take the full functional form too seriously but rather view the sine functions as a convenient place-holder for a perturbative expansion in higher powers of the K -components. Since there will be other corrections as mentioned above, they could easily dominate most of the expansion terms.

Although the parameters δ and ℓ_0 appear in similar forms, their origins and roles are quite different. The parameter ℓ_0 arises as the coordinate length of a radial edge along which we compute a holonomy. Its size is determined by the embedded graph we act on, as well as the precise form of the Hamiltonian constraint operator understood in the construction. While a Hamiltonian operator does not depend on the embedding and thus ℓ_0 , that dependence would arise in the cause of computing an effective Hamiltonian as the expectation value in a state peaked on a classical geometry. Specifying the classical geometry requires one to partially fix the diffeomorphism gauge; the size of ℓ_0 is then a direct measure for the discreteness of the state in this setting. Also δ measures the discreteness, but it does not refer to the length of any edge. It is associated with curvature components K_φ along spherical symmetry orbits, and there is no room for orbital edges in this reduced model. To understand the meaning of δ , we again have to look at what

it should correspond to in a full, unreduced setting as we did in Sec. 3.3 to discuss the size of inverse triad corrections α . In a fully inhomogeneous setting, there would now be edges along spherical orbits whose lengths correspond to δ . For a configuration which is nearly spherical, there should be a regular distribution of edges forming a lattice on each symmetry orbit. The length of each edge, and thus δ , would decrease with an increasing number of lattice plaquettes \mathcal{N} : $\delta \propto \mathcal{N}^{-1/2}$. In particular, for finer lattices we have $\delta \rightarrow 0$ just as $\ell_0 \rightarrow 0$, approaching the continuum limit.

The precise form of δ depends on the exact state which is approximated by a spherically symmetric one. In particular, the argument shows that δ , unlike ℓ_0 , may be phase-space dependent if geometrical growth is accompanied by a refinement of the lattice such that $\mathcal{N}(E^x)$ depends on E^x , e.g. by a power-law form $\mathcal{N}(E^x) \propto |E^x|^k$. (Note that $4\pi|E^x(x)|$ is the area of a sphere at radius x , and thus coordinate independent. In fact, a densitized triad E^x in one dimension behaves like a scalar.)

In this way, we are naturally led to a refinement scheme of phase-space dependent holonomies where point holonomies associated with K_φ depend on E^x , while K_x -holonomies along the inhomogeneous direction are triad independent. In a reduction to anisotropic but homogeneous models as in [82], this specific form has been shown to imply a dynamical law given by a fundamental difference equation which cannot be implemented equidistantly in minisuperspace variables. Equidistant versions of the difference equation, which would result if holonomies for a connection or extrinsic curvature component depend only on its conjugate triad component, i.e. E^φ for K_φ -holonomies, are not embeddable in a spherically symmetric model. In this way, inhomogeneous models can reduce some of the freedom involved in choosing a refinement scheme for a homogeneous model. Nevertheless, at least a 1-parameter freedom of $\mathcal{N}(E^x) \propto |E^x|^k$, or even a different functional behavior, is left. It is only the direction dependence of \mathcal{N} which is restricted, not the size-dependence. In particular, it is impossible to restrict the corresponding freedom in isotropic models. What we can also see is the fact that spherically symmetric refinement schemes which do not depend on any auxiliary scales can give rise to apparently scale dependent equations in a homogeneous reduction: when reduced to isotropy, a non-trivial refinement scheme can always be expressed by a function $\mathcal{N}(a)$ of the scale factor a . In contrast to E^x , a is coordinate dependent since it rescales if spatial coordinates are multiplied by a constant. The reduction from spherical symmetry thus must automatically introduce a scaling dependent parameter f_0 such that $\mathcal{N}(a)$ depends only on the coordinate independent combination $f_0 a$. This results in a well-defined way of non-trivial refinement schemes with all the freedom as it is realized in spherical symmetry. Moreover, since the scaling dependence arises only in the reduction to homogeneity, it cannot be used as a reliable criterion to rule out refinement schemes if it is applied purely in homogeneous situations.

The lattice refinement behavior is to be expected in any model on general grounds [28, 29]; while a direct derivation of the behavior of $\mathcal{N}(E^x)$ from a full Hamiltonian operator is difficult, one can arrive at some properties and analyze their consequences phenomenologically. For cosmology, such work has been done in [71, 72, 42, 44] and is initiated here for black hole physics. (The interior of the Schwarzschild black hole, which can be formulated as a homogeneous model, has been studied from this perspective in [82, 85, 86].)

4 Corrected LTB models

An LTB reduction at the dynamical quantum level of spherically symmetric systems is difficult because the combined algebra of LTB conditions and constraints, when seen as an extended constrained system, is not purely first class. Although, as mentioned, the classical LTB conditions are preserved by the equations of motion generated by the spherically symmetric Hamiltonian constraint, there is no simple off-shell algebra between these functionals which one could represent on the Hilbert space generated by spherically symmetric spin network states. The various versions of quantum corrected Hamiltonians we have provided so far are thus not yet LTB reduced, although we have already removed the spin connection terms as they drop out in the classical LTB reduction. Moreover, although we did see that the classical LTB conditions can directly be taken over to the kinematical quantum level, such a step is much more complicated when combined with the quantum constraint algebra. If overall consistency with the constraints is required, the LTB conditions themselves may well require quantum corrections, too. In this section, we will be exploring the possibility of LTB-like solutions at a phenomenological effective level, allowing for corrections to constraints as well as the classical LTB conditions.

At this stage, we still have two canonical pairs and two smeared constraints (the diffeomorphism and corrected Hamiltonian constraint). The corrected constraints in this form are automatically consistent (i.e. first class) since the absence of the spin connection terms implies the absence of spatial derivatives in H_{grav} ; the Hamiltonian constraints thus commute with themselves. Even if we add the non-dynamical dust contribution $H_{\text{dust}} = F'/2G$ in terms of the mass function $F(x)$, the system remains consistent. We have dropped the spin connection terms in anticipation of the imposition of LTB conditions, which solve the diffeomorphism constraint identically and thus show that the Abelian Poisson bracket $\{H[N], H[M]\} = 0$, realized even in the quantum corrected case, is correct. With such an algebra, the LTB form allows us to discuss the anomaly issue more easily. However, there is still a potential anomaly problem, whose solution allows us to draw feedback for quantizations of the Hamiltonian constraint: the reduction to constraints of LTB form is consistent only if there are LTB-like conditions, relating E^φ to $(E^x)'$ and K'_φ to K_x , which are preserved by the quantum corrected spherically symmetric constraints. The requirement of preserved LTB conditions will, as we will see, restrict the form of quantum corrections in different terms of the constraints.

4.1 Consistent LTB reductions

To derive equations of motion for the metric component R left as the only degree of freedom in an LTB metric, we eliminate K_φ and K_x in favor of \dot{E}^φ and \dot{E}^x using the equations of motion $\dot{E}^I = \{E^I, H\}$ where $I \in \{\varphi, x\}$. To evaluate these expressions we make use of the canonical Poisson bracket relations $\{K_x(x), E^x(y)\} = 2G\delta(x - y)$ and

$\{K_\varphi(x), E^\varphi(y)\} = G\delta(x - y)$ as they follow from (26), such that

$$K_\varphi = \frac{\dot{E}^x}{2\sqrt{|E^x|}} \quad , \quad K_x = \frac{1}{\sqrt{|E^x|}} \left(\dot{E}^\varphi - \frac{\dot{E}^x E^\varphi}{2E^x} \right) \quad (52)$$

for the classical constraint.

The key problem now is that (28) combined with (33) is no longer preserved by the evolution equations generated by (49) or (50) for $\alpha \neq 1$, as can directly be checked. If these equations were consistent, one could eliminate the variable E^φ in favor of E^x in all equations of motion, which is then expressed as $E^x = R^2$. (From now on we assume $E^x > 0$ without loss of generality for the applications we are interested in.) Thus, a complete set of equations given by the Hamiltonian constraint for \dot{R} and the second order evolution equation for R would be obtained. When the LTB conditions are not preserved, however, the Hamiltonian constraint equation for R will not be preserved by the evolution equation.

Before deriving quantum corrected equations for R , we thus have to find LTB conditions suitable for the quantum corrected dynamics. The main conditions are (i) that they reduce to the classical LTB conditions when quantum corrections vanish, (ii) that they still solve the uncorrected diffeomorphism constraint identically as this is necessary for a consistent constraint algebra, and (iii) that they be preserved by the quantum corrected evolution equations. Condition (ii) is also motivated by the fact that finite diffeomorphisms are represented in loop quantum gravity directly by the action they generate on phase space functions without requiring any quantum corrections.

4.1.1 Inverse triad corrections: first version

In agreement with the diffeomorphism constraint, we make the ansatz

$$(E^x)' = 2f(E^x)E^\varphi \quad , \quad K'_\varphi = f(E^x)K_x \quad (53)$$

where, as indicated, $f(E^x)$ is assumed to depend only on E^x in algebraic form. This function will be determined by demanding that the new LTB conditions are preserved in time by (49). Writing the first constraint in the smeared form $C_{\text{LTB}} = \int dx \mu(x) (2f(E^x)E^\varphi - (E^x)')$, we require that the Poisson bracket $\{C_{\text{LTB}}, \int dy H_{\text{grav}}^{(I)}\}$, which evaluates to

$$\int dz \mu(z) \left(-4K_\varphi E^\varphi \sqrt{E^x} \frac{df}{dE^x} + 2K'_\varphi \sqrt{E^x} + \frac{K_\varphi (E^x)'}{\sqrt{E^x}} - \frac{2f\alpha K_\varphi E^\varphi}{\sqrt{E^x}} - 2fK_x \sqrt{E^x} \right) , \quad (54)$$

vanishes for all $\mu(x)$. Using (53) to remove the derivative terms we get

$$\int dz \mu(z) \left(-4K_\varphi E^\varphi \sqrt{E^x} \frac{df}{dE^x} + \frac{2fK_\varphi E^\varphi}{\sqrt{E^x}} - \frac{2f\alpha K_\varphi E^\varphi}{\sqrt{E^x}} \right) . \quad (55)$$

For this to vanish for all μ , the integrand must vanish which therefore gives the differential equation

$$f(1 - \alpha) = 2E^x \frac{df}{dE^x} \quad (56)$$

for $f(E^x)$ which, for α as in (48), is solved by

$$f(E^x) = \frac{c_1 \sqrt{E^x} e^{-\alpha/2}}{\left(\sqrt{E^x} + \sqrt{E^x - \gamma \ell_{\text{P}}^2/2}\right)^{1/2} \left(\sqrt{E^x} + \sqrt{E^x + \gamma \ell_{\text{P}}^2/2}\right)^{1/2}}. \quad (57)$$

for $E^x > \gamma \ell_{\text{P}}^2/2$ and

$$f(E^x) = \frac{c_2 \sqrt{E^x} \exp\left(-\frac{1}{2}\alpha + \frac{1}{2} \arctan\left(\sqrt{E^x/(\gamma \ell_{\text{P}}^2/2 - E^x)}\right)\right)}{\sqrt{\sqrt{E^x} + \sqrt{E^x + \gamma \ell_{\text{P}}^2/2}}} \quad (58)$$

for $E^x < \gamma \ell_{\text{P}}^2/2$. The constant c_1 is fixed by demanding that in the limit $E^x \rightarrow \infty$ the corrected LTB conditions should go to their classical form. To ensure $f(E^x) \rightarrow 1$ in the classical limit we have $c_1 = 2\sqrt{e}$. The functions f and α then have similar fall-off behaviors at large E^x : $f(E^x) \sim 1 + 2^{-7}\gamma^2 \ell_{\text{P}}^4 (E^x)^{-2} + \dots$ while $\alpha(E^x) \sim 1 + 2^{-5}\gamma^2 \ell_{\text{P}}^4 (E^x)^{-2} + \dots$. The second constant c_2 is determined by continuity at $E^x = \gamma \ell_{\text{P}}^2/2$, which gives $c_2 = 2^{5/4} e^{1/2 - \pi/4} \gamma^{-1/4} \ell_{\text{P}}^{-1/2}$. It is easy to check that with this form for $f(E^x)$ the other LTB condition, $K'_\varphi = f(E^x)K_x$, is also preserved in time.

We now eliminate the connection components from the Hamiltonian in favor of the triad components E^x and E^φ using the equations of motion which give

$$K_\varphi = \frac{\dot{E}^x}{2\sqrt{E^x}} \quad , \quad K_x = \frac{1}{\sqrt{E^x}} \left(\dot{E}^\varphi - \alpha \frac{\dot{E}^x E^\varphi}{2E^x} \right). \quad (59)$$

We then further eliminate E^φ using the new LTB conditions to obtain

$$H_{\text{grav}}^{(I)} = -\frac{1}{2G} \left(\frac{\alpha(\dot{E}^x)^2 (E^x)'}{8f(E^x)^{3/2}} + \frac{\dot{E}^x (\dot{E}^x)'}{2f\sqrt{E^x}} - \frac{(\dot{E}^x)^2 (E^x)'}{4f(E^x)^{3/2}} \right). \quad (60)$$

The total Hamiltonian constraint $H_{\text{grav}}^{(I)} + H_{\text{dust}} = 0$ then becomes

$$\frac{\alpha(\dot{E}^x)^2 (E^x)'}{8f(E^x)^{3/2}} + \frac{\dot{E}^x (\dot{E}^x)'}{2f\sqrt{E^x}} - \frac{(\dot{E}^x)^2 (E^x)'}{4f(E^x)^{3/2}} - F' = 0 \quad (61)$$

with the given E^x -dependence of f and α .

To obtain the evolution equation we take a time derivative of the first equation in (59) to obtain

$$\dot{K}_\varphi = \frac{2E^x \ddot{E}^x - (\dot{E}^x)^2}{4|E^x|^{3/2}}. \quad (62)$$

Since \dot{K}_φ is also determined by $\dot{K}_\varphi = \{K_\varphi, H_{\text{grav}}^{(I)}\} = -\alpha K_\varphi^2 / 2\sqrt{E^x}$ we have

$$4E^x \ddot{E}^x - (2 - \alpha)(\dot{E}^x)^2 = 0 \quad (63)$$

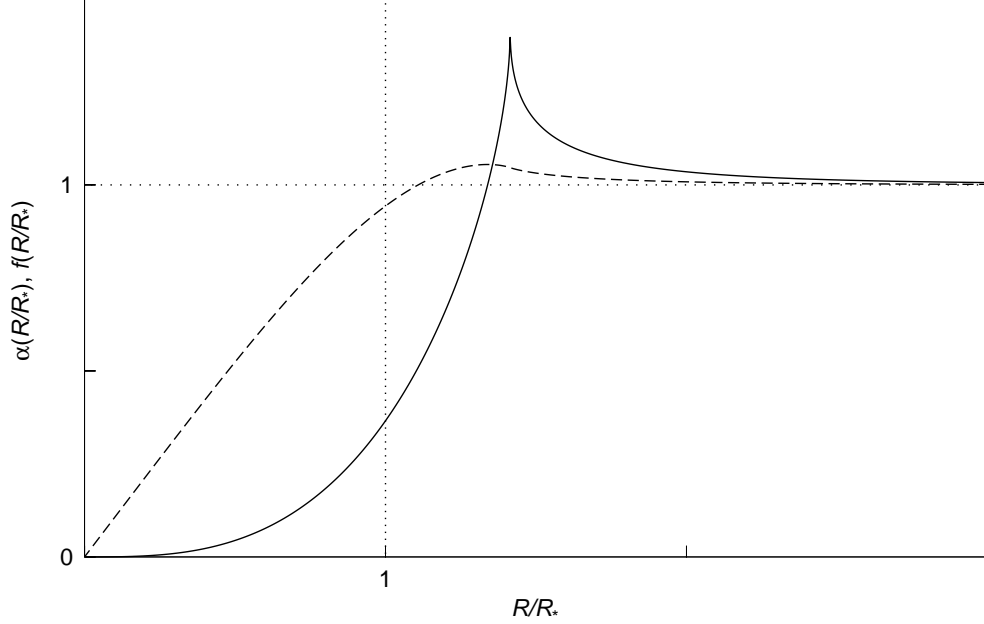


Figure 1: The correction functions $\alpha(R)$ (solid) and $f(R)$ (dashed) where R is taken relative to $R_* := \sqrt{\gamma/2}\ell_P$.

We note that in this derivation of the evolution equation, $f(E^x)$ does not appear anywhere. Nevertheless, its form is important for the mutual consistency of the evolution equation (63) and the Hamiltonian constraint equation (61).

We can now write everything in terms of R using the relation $E^x = R^2$:

$$\alpha(R) = 2 \frac{\sqrt{|R^2 + \gamma\ell_P^2/2|} - \sqrt{|R^2 - \gamma\ell_P^2/2|}}{\gamma\ell_P^2} R \quad (64)$$

$$f(R) = \begin{cases} \frac{2R \exp(\frac{1}{2}(1-\alpha(R)))}{(R + \sqrt{R^2 - \gamma\ell_P^2/2})^{1/2} (R + \sqrt{R^2 + \gamma\ell_P^2/2})^{1/2}} & \text{for } R > \sqrt{\gamma/2}\ell_P \\ \frac{2^{5/4} R \exp(\frac{1}{2}(1-\alpha(R)) + \frac{1}{2} \arctan(\sqrt{R^2/(\gamma\ell_P^2/2 - R^2)}) - \pi/4)}{\gamma^{1/4} \sqrt{\ell_P} \sqrt{R + \sqrt{R^2 + \gamma\ell_P^2/2}}} & \text{for } R < \sqrt{\gamma/2}\ell_P \end{cases} \quad (65)$$

These functions are shown in Fig. 1. The first order equation (61) can be written as

$$\dot{R}^2 R' (\alpha(R) - 1) + 2R \dot{R} \dot{R}' + \dot{R}^2 R' = f(R) F' \quad (66)$$

and the evolution equation is

$$2R \ddot{R} + \dot{R}^2 + (\alpha(R) - 1) \dot{R}^2 = 0. \quad (67)$$

These equations can explicitly be seen to be consistent upon using the differential relation (56) between f and α .

4.1.2 Inverse triad corrections: second version

Starting from (50), which gives equations of motion

$$\dot{E}^x = 2\alpha K_\varphi \sqrt{E^x} \quad , \quad \dot{E}^\varphi = \alpha K_\varphi \frac{E^\varphi}{\sqrt{E^x}} + \alpha K_x \sqrt{E^x} \quad (68)$$

$$\dot{K}_x = \alpha K_\varphi^2 \frac{E^\varphi}{2(E^x)^{3/2}} - \alpha K_\varphi \frac{K_x}{\sqrt{E^x}} - \frac{d\alpha}{dE^x} K_\varphi^2 \frac{E^\varphi}{\sqrt{E^x}} - 2 \frac{d\alpha}{dE^x} K_\varphi K_x \sqrt{E^x} \quad (69)$$

$$\dot{K}_\varphi = -\alpha \frac{K_\varphi^2}{2\sqrt{E^x}} \quad (70)$$

we can proceed similarly. Also with these equations, the classical LTB conditions will not be preserved such that the reduction would be inconsistent. However, one can verify that the corrected LTB conditions

$$E^\varphi = \frac{1}{2\alpha} (E^x)' \quad , \quad \alpha K_x = K'_\varphi \quad (71)$$

are preserved as before.

Proceeding with these equations of motion and LTB conditions, we obtain

$$\left(\frac{\dot{R}^2 R}{\alpha^2} \right)' - F' = 0 \quad (72)$$

as the Hamiltonian constraint equation in the presence of dust. Thus, the corrected equation for R is

$$\dot{R}^2 R = \alpha^2 (F(r) + c(t)) . \quad (73)$$

The evolution equation derived via \dot{K}_φ is

$$2R\ddot{R} + \dot{R}^2 = 2 \frac{d \log \alpha}{d \log R} \dot{R}^2 \quad (74)$$

with a quantum correction on the right hand side. Taking a time derivative of (73), using $\dot{F} = 0$ and eliminating F from the resulting equation via (73) indeed produces (74) provided $c(t) = c = \text{const}$. Thus, the system is consistent, and the freedom of $c(t)$ in (73) is reduced to a constant which can be absorbed in the mass function.

4.1.3 Holonomy corrections

We now look for a consistent formulation with corrections due to holonomy effects. It turns out that the Hamiltonian (51) leads to equations which are algebraically complicated to handle. To avoid technical difficulties, we first look at a Hamiltonian where K_φ appears via the function $(\gamma\delta)^{-1} \sin(\gamma\delta K_\varphi)$ but K_x has its classical appearance (i.e. the continuum limit $\ell_0 \rightarrow 0$ has been taken):

$$H_{\text{grav}}^{(IIIa)} = -\frac{1}{2G} \left(\frac{\sin^2(\gamma\delta K_\varphi)}{\gamma^2 \delta^2} \frac{E^\varphi}{\sqrt{E^x}} + 2 \frac{\sin(\gamma\delta K_\varphi)}{\gamma\delta} K_x \sqrt{E^x} \right) . \quad (75)$$

This describes holonomy corrections in regions where K_φ is large but K_x remains small, or for states with a dense radial lattice such that ℓ_0 is small. Again, the classical LTB conditions would not be preserved, and therefore we look for an alternative of the form

$$(E^x)' = 2g(K_\varphi)E^\varphi \quad , \quad K'_\varphi = g(K_\varphi)K_x \quad (76)$$

compatible with the diffeomorphism constraint, where $g(K_\varphi)$ is assumed to depend only on K_φ . As before, this dependence will be self-consistently verified by demanding that the new LTB conditions are preserved in time: $\{\int dx\mu(x)(2gE^\varphi - (E^x)'), \int dyH_{\text{grav}}^{(IIIa)}\} = 0$ for all $\mu(x)$. This Poisson bracket evaluates to

$$\int dz\mu(z) \left(\frac{\sin^2(\gamma\delta K_\varphi)}{\gamma^2\delta^2} \frac{E^\varphi}{\sqrt{E^x}} \frac{dg}{dK_\varphi} - 2g \frac{\sin(\gamma\delta K_\varphi) \cos(\gamma\delta K_\varphi)}{\gamma\delta} \frac{E^\varphi}{\sqrt{E^x}} \right. \\ \left. - 2g \cos(\gamma\delta K_\varphi) K_x \sqrt{E^x} + 2 \cos(\gamma\delta K_\varphi) K'_\varphi \sqrt{E^x} + \frac{\sin(\gamma\delta K_\varphi) (E^x)'}{\gamma\delta \sqrt{E^x}} \right). \quad (77)$$

Substituting for $(E^x)'$ and K'_φ from the corrected LTB conditions, we have

$$\int dz\mu(z) \left(\frac{\sin^2(\gamma\delta K_\varphi)}{\gamma^2\delta^2} \frac{E^\varphi}{\sqrt{E^x}} \frac{dg}{dK_\varphi} - 2g \frac{\sin(\gamma\delta K_\varphi) \cos(\gamma\delta K_\varphi)}{\gamma\delta} \frac{E^\varphi}{\sqrt{E^x}} \right. \\ \left. + \frac{2g \sin(\gamma\delta K_\varphi)}{\gamma\delta} \frac{E^\varphi}{\sqrt{E^x}} \right). \quad (78)$$

For this to be zero for all μ , the integrand must vanish which implies the differential equation

$$\frac{\sin(\gamma\delta K_\varphi)}{\gamma\delta} \frac{dg}{dK_\varphi} = 2(\cos(\gamma\delta K_\varphi) - 1)g \quad (79)$$

solved by

$$g(K_\varphi) = c \cos^4(\gamma\delta K_\varphi/2). \quad (80)$$

The classical limit $g \rightarrow 1$ for $\delta \rightarrow 0$ fixes the constant of integration $c = 1$. One can check that the other LTB condition is consistent with this choice for $g(K_\varphi)$.

As before we now eliminate the connection components in favor of the triad components. The equations of motion give

$$\dot{E}^x = \frac{2 \sin(\gamma\delta K_\varphi)}{\gamma\delta} \sqrt{E^x} \quad (81)$$

$$\dot{E}^\varphi = \frac{\sin(\gamma\delta K_\varphi) \cos(\gamma\delta K_\varphi)}{\gamma\delta} \frac{E^\varphi}{\sqrt{E^x}} + \cos(\gamma\delta K_\varphi) K_x \sqrt{E^x}. \quad (82)$$

We use (81) to express the (co)sine function in terms of E^x :

$$\sin(\gamma\delta K_\varphi) = \frac{\gamma\delta}{2} \frac{\dot{E}^x}{\sqrt{E^x}} \quad , \quad \cos(\gamma\delta K_\varphi) = \pm \sqrt{1 - \frac{\gamma^2\delta^2}{4} \frac{(\dot{E}^x)^2}{E^x}} \quad (83)$$

and solve (82) for

$$K_x = \frac{1}{\cos(\gamma\delta K_\varphi)\sqrt{E^x}} \left(\dot{E}^\varphi + \frac{\sin(\gamma\delta K_\varphi) \cos(\gamma\delta K_\varphi)}{\gamma\delta} \frac{E^\varphi}{\sqrt{E^x}} \right). \quad (84)$$

After substituting for the sine and the cosine (choosing the plus sign in the cosine), this can be written as

$$K_x = \left(\dot{E}^\varphi - \frac{\dot{E}^x E^\varphi}{2E^x} \sqrt{1 - \frac{\gamma^2 \delta^2 (\dot{E}^x)^2}{4 E^x}} \right) \left(E^x - \frac{\gamma^2 \delta^2 (\dot{E}^x)^2}{4} \right)^{-1/2}. \quad (85)$$

Substituting for K_x and $\sin(\gamma\delta K_\varphi)$ back in the expression for the Hamiltonian (75) we have

$$H_{\text{grav}}^{(IIIa)} = -\frac{1}{2G} \left(\frac{\dot{E}^x \dot{E}^\varphi}{\sqrt{E^x - \frac{1}{4}\gamma^2 \delta^2 (\dot{E}^x)^2}} - \frac{(\dot{E}^x)^2 E^\varphi}{4(E^x)^{3/2}} \right). \quad (86)$$

The new LTB condition $E^\varphi = (E^x)' / 2g = (E^x)' / 2 \cos^4(\gamma\delta K_\varphi / 2)$ allows us to eliminate E^φ using (83):

$$\cos^4(\gamma\delta K_\varphi / 2) = \frac{1}{4} \left(1 + \sqrt{1 - \frac{\gamma^2 \delta^2 (\dot{E}^x)^2}{4 E^x}} \right)^2 \quad (87)$$

which gives

$$E^\varphi = \frac{2(E^x)'}{\left(1 + \sqrt{1 - \frac{1}{4}\gamma^2 \delta^2 \frac{(\dot{E}^x)^2}{E^x}} \right)^2}. \quad (88)$$

Substituting for E^φ and its time derivative in (86) implies

$$\begin{aligned} -2GH_{\text{grav}}^{(IIIa)} &= \frac{2\dot{E}^x (\dot{E}^x)'}{(E^x)^{\frac{1}{2}} \left(1 + \sqrt{1 - \frac{1}{4}\gamma^2 \delta^2 \frac{(\dot{E}^x)^2}{E^x}} \right)^2 \sqrt{1 - \frac{1}{4}\gamma^2 \delta^2 \frac{(\dot{E}^x)^2}{E^x}}} - \frac{(\dot{E}^x)^2 (E^x)'}{2(E^x)^{\frac{3}{2}} \left(1 + \sqrt{1 - \frac{1}{4}\gamma^2 \delta^2 \frac{(\dot{E}^x)^2}{E^x}} \right)^2} \\ &+ \frac{\gamma^2 \delta^2 \dot{E}^x (E^x)' (2E^x \dot{E}^x \ddot{E}^x - (\dot{E}^x)^3)}{2(E^x)^{\frac{5}{2}} \left(1 + \sqrt{1 - \frac{1}{4}\gamma^2 \delta^2 \frac{(\dot{E}^x)^2}{E^x}} \right)^3 \left(1 - \frac{1}{4}\gamma^2 \delta^2 \frac{(\dot{E}^x)^2}{E^x} \right)}. \end{aligned}$$

We now derive the evolution equation consistent with (86). On the one hand, we have the equation of motion

$$\dot{K}_\varphi = -\{K_\varphi, H_{\text{grav}}^{(IIIa)}\} = \frac{\sin^2(\gamma\delta K_\varphi)}{2\gamma^2 \delta^2} \frac{1}{\sqrt{E^x}} \quad (89)$$

and, on the other hand, differentiating (81) with respect to time gives

$$\dot{K}_\varphi = \frac{1}{2 \cos(\gamma\delta K_\varphi)} \left(\frac{\ddot{E}^x}{\sqrt{E^x}} - \frac{(\dot{E}^x)^2}{2(E^x)^{3/2}} \right). \quad (90)$$

Combining these two equations and writing everything in terms of R , we have

$$2R\ddot{R} + \dot{R}^2\sqrt{1 - \gamma^2\delta^2\dot{R}^2} = 0. \quad (91)$$

The evolution equation can now be used to eliminate the second time derivative of E^x from $H_{\text{grav}}^{(IIIa)}$, which together with $E^x = R^2$ and in combination with the matter part provides the Hamiltonian constraint equation

$$4\dot{R}^2R'\sqrt{1 - \gamma^2\delta^2\dot{R}^2} + 8R\dot{R}\dot{R}' = F' \left(1 + \sqrt{1 - \gamma^2\delta^2\dot{R}^2} \right)^2 \sqrt{1 - \gamma^2\delta^2\dot{R}^2}. \quad (92)$$

We note that in the limit $\delta \rightarrow 0$ we recover the classical equation which also justifies the choice of plus sign in (83).

Finally, we could use a Hamiltonian where only K_x has been replaced by periodic functions,

$$H_{\text{grav}}^{(IIIb)} = -\frac{1}{2G} \left(\frac{K_\varphi^2 E^\varphi}{\sqrt{E^x}} + 2K_\varphi \frac{\sin(\gamma K_x \ell_0)}{\gamma \ell_0} \sqrt{E^x} \right). \quad (93)$$

In this case, however, the corrected LTB conditions will take a more complicated form because correction functions will have to depend on all the phase space variables, as one can check by making an ansatz as before. We leave this complicated case open for future work and proceed with a general discussion and applications of the consistent versions found.

4.2 Discussion

We have provided several cases of consistent equations of motion for the variables of a metric of LTB form, but with dynamics carrying corrections as they are expected from loop quantum gravity. While we have discussed inverse triad and one form of holonomy corrections separately, they can be seen to be combined consistently simply in a multiplicative form of the correction functions in the LTB conditions. For instance, the first version of inverse triad corrections and the holonomy correction we used can be consistently combined in this way to result in a Hamiltonian constraint equation

$$\alpha\dot{R}^2R' + \frac{2R\dot{R}\dot{R}'}{\sqrt{1 - \gamma^2\delta^2\dot{R}^2}} = f_\delta F' \quad (94)$$

where $f_\delta[R] = f(R) \left(1 + \sqrt{1 - \gamma^2\delta^2\dot{R}^2} \right)^2$ together with the evolution equation

$$2R\ddot{R} = -\alpha\dot{R}^2\sqrt{1 - \gamma^2\delta^2\dot{R}^2}. \quad (95)$$

With the second version of inverse triad corrections, we have

$$\begin{aligned}
& -4\alpha^2 \dot{R}^2 R' \sqrt{1 - \frac{\gamma^2 \delta^2 \dot{R}^2}{\alpha^2}} - 4\alpha^2 \dot{R}^2 R' - 4\gamma^2 \delta^2 \dot{R}^4 R' + 8\alpha^2 R \dot{R} \dot{R}' \left(1 + \sqrt{1 - \frac{\gamma^2 \delta^2 \dot{R}^2}{\alpha^2}} \right) \\
& + \frac{8\alpha^2 R^2 \dot{R}^2 R'}{\sqrt{R^4 - (\gamma \ell_p^2/2)^2}} \left(1 + \sqrt{1 - \frac{\gamma^2 \delta^2 \dot{R}^2}{\alpha^2}} \right) = F' \alpha^4 \left(1 + \sqrt{1 - \frac{\gamma^2 \delta^2 \dot{R}^2}{\alpha^2}} \right)^3 \sqrt{1 - \frac{\gamma^2 \delta^2 \dot{R}^2}{\alpha^2}}
\end{aligned} \tag{96}$$

and

$$2R\ddot{R} = 2\dot{R}^2 - \frac{2R^2 \dot{R}^2}{\sqrt{R^4 - (\gamma \ell_p^2/2)^2}} - \dot{R}^2 \sqrt{1 - \frac{\gamma^2 \delta^2 \dot{R}^2}{\alpha^2}}. \tag{97}$$

While general properties of an LTB reduction allowed us to keep the constraints consistent without severe limitations on quantum correction functions, consistency conditions did remain. The remaining constraints automatically form a first class system provided that the Hamiltonian constraint is free of spatial derivatives, which is realized if spin connection terms (or the 3-dimensional Ricci curvature) drop out as it happens under the classical LTB conditions. The consistency conditions arose at the level of formulating the LTB conditions, because the classical ones are no longer preserved under evolution corresponding to quantum corrected constraints. We thus corrected the LTB conditions, too, such that in their new form they were preserved under the quantum corrected equations of motion as they are generated by a Hamiltonian whose spin connection contribution vanishes.

With these conditions we are still identically satisfying the classical diffeomorphism constraint and thus no new anomalies in the constraint algebra can arise. However, the corrected LTB conditions do not make the classical spin connection Γ_φ equal -1 , which was assumed in the simplified classical Hamiltonians such as (49). Thus, to be fully consistent we must assume that the expressions containing the spin connection themselves carry quantum corrections and read $f(E^x)\Gamma_\varphi^{(I)} = -(E^x)'/2E^\varphi$ for the equations in Sec. 4.1.1, $\alpha(E^x)\Gamma_\varphi^{(II)} = -(E^x)'/2E^\varphi$ for Sec. 4.1.2 and $g(K_\varphi)\Gamma_\varphi^{(IIIa)} = -(E^x)'/2E^\varphi$ in Sec. 4.1.3. Thus, for consistency additional corrections of this form must arise in the terms of the Hamiltonian constraint containing the spin connection in such a way that they vanish after imposing the quantum corrected LTB conditions.

That the spin connection terms carry their own corrections is a reasonable expectation: There are inverse triad components and, in a loop quantization, the spin connection is rather indirectly expressed via A_a^i and $\gamma K_a^i = A_a^i - \Gamma_a^i \propto \{A_a^i, \{H^{(E)}, V\}\}$ using the Euclidean part $H^{(E)}$ of the Hamiltonian constraint [77]. Corrections are thus expected from the inverse triad as well as from holonomies. The specific form is difficult to determine because the full theory does not provide operators for the non-covariant spin connection components, but as demonstrated here it can be derived and justified by the production of a consistent set of equations. In fact, if such corrections occur, our equations provide a fully consistent LTB system. In this way, consistency determines what further quantum

corrections must be entailed by a primary correction such as α . Since not all corrections in a Hamiltonian can equally easily be computed, independent consistency considerations provide useful relations between different terms. For instance, the spin connection is more difficult to quantize than $1/E^x$, and its corrections can thus more easily be found via consistency.

An important physical implication is that this suggests additional effects because the space-time metric (18) is no longer just corrected by different solutions for $R(t)$ solving the corrected constraint and evolution equations, but also by an additional pre-factor in terms of α , f or g in front of $L^2 \propto (R')^2$ which is no longer exactly $(R')^2$. This would, for instance, affect the appearance of horizons.

5 Applications

Our focus in this paper for applications of the above equations is the fate of the classical singularity which appears at $R = 0$. There are two possibilities for how such a singularity could be avoided in effective equations. Dynamically, $R(t, x)$ may be bounded away from zero for all x , in which case the behavior shown would be comparable to a cosmological bounce. This can sometimes occur if isotropic cosmological models exhibiting a bounce are matched to a spherically symmetric outside region in a generalized Oppenheimer–Snyder manner [87]. The outright spherically symmetric situation studied here is, however, subject to different corrected equations and so one has to provide a new analysis.

The second possibility is that the value $R = 0$ is assumed, but that this does not result in a singular space-time just as Minkowski space in polar coordinates has $R = 0$ at $x = 0$. If $R = 0$ occurs, one thus has to proceed with a more detailed analysis to understand the space-time neighborhood of the region where $R = 0$.

Compared to homogeneous equations, this problem is of a new quality. As we have seen, there is a non-trivial anomaly problem which we were able to resolve in different versions of quantum corrected LTB models. The presence of consistency conditions, which do not arise in homogeneous models because they are subject to just a single constraint, makes the form of quantum corrections more restricted. Thus, several different terms in the constraints must receive quantum corrections in a way closely related to each other. Still, we have explicitly shown that non-trivial quantum corrections are allowed.

In addition to the anomaly issue, spatial inhomogeneity allows different types of singularities in classical general relativity. In particular, not just spacelike singularities can occur as in homogeneous models, but also null [55, 58] or timelike ones [88]. This has interesting general ramifications concerning the consistency of quantum gravity in the sense of allowing stable ground states, as discussed in [89], and it underlines the interest in inhomogeneous models. In what follows, we present an initial analysis based on analytical as well as numerical methods.

5.1 Analytical properties

If there is a “bounce” where the area radius R attains a non-zero minimum value, we have $\dot{R} = 0$ which can be substituted in the above equations to check the possibility for this to happen in quantum gravity. From Eq. (66) (for the first version of inverse triad corrections) or Eq. (92) (for holonomy corrections) as well as the two combinations (94) and (96) we can immediately see that this is not possible unless we drop the condition $F' > 0$ which classically avoids shell-crossing singularities. Thus, we either have to drop this condition, possibly taking into account quantum geometry corrections in the matter sector, or retain the non-bouncing behavior of the classical models. For the second version of inverse triad corrections, Eq. (73), we would require $F = 0$ at the bounce, which looks difficult to achieve in a generic collapse model. (Conditions on F may be avoided if \dot{R}' diverges where $\dot{R} = 0$, but this does not appear generic.)

There does not appear to be a simple conclusion about bounces as they occur, e.g., in homogeneous models. We are looking at specific regimes and certain types of quantum corrections which, by themselves, may make a bounce difficult to occur. Moreover, we have restricted the analysis to marginal models, which classically includes spatially flat Friedmann–Robertson–Walker models as the interior region of Oppenheimer–Snyder collapse, but not isotropic models with positive spatial curvature. The latter (or scalar matter with negative potential [90]) would be required for a bounce based on inverse triad corrections [91]. There is thus no contradiction with known matching results based on isotropic interiors [87], but the fact that a bounce does not follow straightforwardly, compared to the relative ease by which this can be obtained in isotropic models, may also be taken as a warning sign concerning the robustness of homogeneous bounces.

Similarly, we have considered holonomy corrections only of a special form which made the analysis more manageable. Holonomy corrections give rise to bounces more generally than inverse triad corrections [92, 93, 30, 33]. One could thus expect that a full treatment of holonomy corrections should give rise to general bounces also in LTB models. However, even though we did not do such an analysis, such a bounce cannot be generic for the following reason: simply choosing a fine spatial graph and thus small enough ℓ_0 makes the holonomy corrections studied here the relevant ones. Since these corrections do not provide an automatic bounce, a bounce cannot be generic in this inhomogeneous system. Finally, there is a third effect due to quantum variables which provides corrections in effective equations. Also this has not been included here, but it is unlikely to result in a general bounce given that it does not do so in isotropic models (where it could even prevent a bounce which would otherwise occur based on holonomy corrections [32, 33]). We thus conclude that singularities in LTB systems do not appear to be resolved by bounces.

5.1.1 Corrected LTB equations as cosmological models

As the simplest case, we first consider a vacuum solution where, in the absence of dust, $F' = 0$ must be satisfied. If $R' \neq 0$ holds, $R = R(x)$, i.e. a static configuration, is a trivial solution to any of the corrected equations (66), (73) and (92). While this corresponds

to the classical Minkowski space solution, since $R(x)$ can then easily be introduced as a coordinate instead of x , there are quantum corrections for small R : Our corrected LTB metric, using $L = R'/f(R)$ for (66) to be specific, reads

$$ds^2 = -dt^2 + \frac{dR^2}{f(R)^2} + R^2(d\vartheta^2 + \sin^2\vartheta d\varphi^2) \quad (98)$$

which asymptotically presents Minkowski space. As we will discuss in more detail below, the appearance of $f(R)$ shows that quantum effects originating in the spatial discreteness of loop quantum gravity spoil some of the exact symmetries such as spatial homogeneity known to exist in classical solutions.

If there is dust, it is of interest to see whether we can have a Friedmann solution in this system. For this we choose x such that it coincides with the circumferential radius at $t = 0$, and make an ansatz of the form $R(t, x) = a(t)x$. If such a solution exists, as it does in the classical case, the LTB metric reduces to a Friedmann–Robertson–Walker one where a is identified with the scale factor. The dust density profile then becomes

$$f(x)F' = 8\pi G\epsilon_0 x^2 \quad (99)$$

where ϵ_0 is the initial uniform density. (According to our general choice of $R(0, x) = x$, the scale factor is normalized to $a_0 = 1$ at $t = 0$ in the cosmological context.) Substituting this into Eq. (66), we have

$$\dot{a}^2 a = \frac{8\pi G\epsilon_0}{3 + (\alpha(ax) - 1)} \frac{f(ax)}{f(x)}. \quad (100)$$

The left-hand side depends only on t while the right-hand side depends non-trivially on ax . Hence, the corrected LTB system does not admit a solution of Friedmann form.

There is an additional effect which prevents Friedmann solutions for the corrected equations, because our LTB form of the metric receives quantum corrections, too, as a consequence of consistency. The corrected LTB metrics have coefficient $L = R'/f(R)$ in the case of $H^{(I)}$, and $L = R'/\alpha(R)$ in the case of $H^{(II)}$. This changes the metric in addition to the corrected dynamics of the metric component R . In particular, the metrics are no longer homogeneous because of the non-trivial R -dependence. If we were interested in spatial volumes of finite regions in constant t slices, for an approximate solution of the form $R = a(t)x$ they would become $V = 4\pi a^3 \int dx x^2/f(ax)$ and $V = 4\pi a^3 \int dx x^2/\alpha(ax)$, respectively. This illustrates an interesting difference between these two cases which both come from inverse triad corrections: for $f(ax)$, we have the small- x expansion $f(ax) \propto ax + O(a^2 x^2)$, while for α it reads $\alpha(ax) \propto a^3 x^3 + O(a^4 x^4)$. Thus, in the first case the spatial volumes vanish at $a = 0$ as in the classical case, while the second case implies diverging volumes $V \sim \int x^{-1} dx$ even of finite regions near $a = 0$. This suggests further implications of the behavior near a classical singularity, which due to the required inhomogeneity do not appear easy to discern.

5.1.2 Effective densities

As a further consequence of corrections, we note that the mass function $F(x)$ is no longer directly related to the Misner–Sharp mass. We need to distinguish the latter from the dust mass which can be defined as

$$M(x) = \frac{F(x)}{2G}. \quad (101)$$

The asymptotic value $M_{\text{dust}} = \lim_{x \rightarrow \infty} M(x)$ corresponds to the total mass of dust. The Misner–Sharp mass, on the other hand, now takes the form

$$m = \frac{R}{2} \left(1 - \left(\frac{R'}{L} \right)^2 + \dot{R}^2 \right) \quad (102)$$

whose expression changes for the corrected LTB conditions because this affects the relation between R' and L . From the corrected mass, we can then derive an effective density $\epsilon = m'/4\pi GR^2 R'$. For instance, for the condition consistent with $H_{\text{grav}}^{(I)}$ we have a Misner–Sharp mass

$$m^{(I)} = \frac{1}{2}R(1 - f^2 + \dot{R}^2) = m_{\text{class}} - \frac{1}{2}R(f^2 - 1) \quad (103)$$

which, upon using (66), leads to an effective density

$$\epsilon^{(I)} = \frac{1}{8\pi GR^2} \left(\frac{f(R)F'}{R'} - (\alpha(R) - 1)(\dot{R}^2 - 2f(R)^2) - (f(R)^2 - 1) \right). \quad (104)$$

Similarly, for the equations following from $H_{\text{grav}}^{(II)}$, we have $m = \frac{1}{2}R(1 - \alpha^2 + \dot{R}^2)$ and thus

$$\epsilon^{(II)} = \frac{1}{8\pi G} \left(\frac{\alpha^2 F'}{R^2 R'} - \frac{\alpha^2 - 1}{R^2} + \frac{2}{\alpha} \frac{d\alpha}{dR} \frac{\dot{R}^2}{R} - 2 \frac{\alpha}{R} \frac{d\alpha}{dR} \right). \quad (105)$$

In particular, in this case the horizon condition $2m = R$ reads $\dot{R}^2 = \alpha^2$, which by the Hamiltonian constraint equation agrees with $\alpha^2 F/R$. Thus, in terms of F the horizon condition $F = R$ is uncorrected in this case, although R as a function of time is corrected compared to the classical behavior.

The correction terms to the effective densities may be nonzero even in vacuum regions devoid of dust. Depending on the regime, they can be positive or negative according to the signs of $\alpha(R) - 1$, $f(R) - 1$ and their derivatives involved.

5.1.3 Existence of self-similar solutions?

The classical equation can rather easily be analyzed using self-similar solutions; see e.g. [50]. One can first write the classical constraint equation as $\dot{R}^2 = F(x)/R$ and then, for the special case of a linear mass function $F(x) = \lambda x$, find an explicit solution for $R(x, t)$ of self-similar form which depends on t only via the function $1 - at/x$ with a constant $a = \frac{3}{2}\sqrt{\lambda}$. For such a self-similar solution, the structure of the singularity has been analyzed in [94].

If we use the second version of inverse triad corrections, this equation is simply changed by multiplying the mass function with $\alpha(R)^2$. Thus, for a linear mass function there is no longer a self-similar solution. One would have to incorporate the new factor by changing the mass function, if a self-similar solution is to be obtained. But this is not straightforward since α depends not on x but on the unknown function R which is to be solved for.

For the first version of inverse triad corrections the equation changes more radically. In this case, we can bring the constraint equation to the form of an integro-differential equation for R ,

$$\left(\frac{dR}{dt}\right)^2 = \frac{1}{R} \int dx f[R(x)] F'(x) - \frac{1}{R} \int dR (\alpha - 1) \left(\frac{dR}{dt}\right)^2. \quad (106)$$

If $\alpha - 1$ is small, one can solve this iteratively by inserting the equation for $(dR/dt)^2$ in the integral:

$$\left(\frac{dR}{dt}\right)^2 = \frac{F(x)}{R} + \frac{1}{R} \int dx (f - 1) F'(x) - \frac{1}{R} \int dR (\alpha - 1) F(x)/R + \dots$$

The difficulty in solving this is that $F(x)$ depends on x rather than R , so we have to know $R(x)$ as a solution and invert it before doing the integration. But this equation already shows qualitatively that the quantum correction makes the solution more non-local, which may prevent the existence of self-similar solutions. Moreover, there will be additional time-dependent effects which do not occur classically. This is so because $R(t, x)$, which we need to know in order to replace x by R in the integrand, also depends on t . Thus, the integrals are really time dependent, which one can understand as replacing the classical $F(x)$ by a new function

$$\begin{aligned} \mathcal{F}(x, t) = & F(x) + \int dx (f - 1) F'(x) - \int dR (\alpha - 1) F(x(R, t))/R \\ & - \int dR (\alpha - 1)/R \int dx (f - 1) F'(x) + \int dR (\alpha - 1)/R \int^R d\tilde{R} (\alpha - 1) F(x(\tilde{R}, t))/\tilde{R} + \dots \end{aligned} \quad (107)$$

appearing on the right hand side of $(dR/dt)^2 = \mathcal{F}(x, t)/R$.

This refers only to the case where $\alpha - 1$ is small, i.e. we have perturbative corrections to the inverse triad effects. It would not allow one to analyze the deeper quantum regime where α differs significantly from one. For this regime we would have to use other techniques, such as the expansions of the following subsection.

However, generally speaking, since the characteristic length scale ℓ_P is explicitly introduced into the corrections, we cannot expect this kind of self-similar solutions, which are called complete self-similar solutions or self-similar solutions of the first kind. With the characteristic length scale, we can only expect incomplete self-similar solutions, e.g. kinematic self-similar solutions in this context; see [95, 96, 97].

5.1.4 Small- x expansion

For $R \gg \sqrt{\gamma}l_{\text{P}}$, $\alpha \rightarrow 1$ and the classical limit is recovered. However, for $R \lesssim \sqrt{\gamma}l_{\text{P}}$, the deviation from classical theory becomes of order unity. Here, deep quantum effects might be revealed by a closer analysis. We point out that such a deep quantum regime is less reliable if only one type of quantum effect is considered. Nevertheless, an analysis of single effects can provide various possibilities and guide further developments. Moreover, the corrections studied here, based on inverse triad and holonomy corrections, can be combined without changing the conclusions.

To have a regular center in an inhomogeneous case we assume that F and R admit the following expansions at the center.

$$F(x) = F_3x^3 + F_4x^4 + \dots \quad , \quad R(t, x) = R_1(t)x + R_2(t)x^2 + \dots \quad (108)$$

where the dots denote higher order terms with respect to x , and F_i are constants but R_i may be t -dependent. In this way, the classical expression for energy density gives an expansion of the form

$$\epsilon(t, x) = \epsilon_0(t) + \epsilon_1(t)x + \epsilon_2(t)x^2 + \dots \quad (109)$$

from $F(x)$ and $R(t, x)$, where $\epsilon_0 = 3F_3/8\pi GR_1^3$. Classically, the lowest order then gives $\dot{R}_1^2 = F_3/R_1$ with solution

$$R_1 = \left(C \pm \frac{3\sqrt{F_3}}{2}t \right)^{2/3} \quad , \quad (110)$$

where C is an arbitrary constant. Hence, for the collapsing case, R_1 monotonically decreases and becomes zero in a finite proper time — the central singularity develops where $\epsilon_0 \rightarrow \infty$. When we choose the radial coordinate x so that $R = x$ at $t = t_0$, we find

$$R_1 = \left(1 \pm \frac{3\sqrt{F_3}}{2}(t - t_0) \right)^{2/3} \quad , \quad (111)$$

and hence, R_1 vanishes at $t = t_s$, where

$$t_s = t_0 \mp \frac{2}{3\sqrt{F_3}} \quad (112)$$

This behavior can be checked also in the presence of quantum corrections to see if anything of the singularity changes. For the first version of inverse triad corrections, we use the small- x behavior

$$\alpha = \left(\frac{2}{\gamma\ell_{\text{P}}^2} \right)^{3/2} R_1^3 x^3 \quad , \quad f = \sqrt{\frac{8e^{1-\pi/2}}{\gamma\ell_{\text{P}}^2}} R_1 x \quad (113)$$

of the correction functions. As a result, if $F(x)$ has a cubic term F_3x^3 as the lowest order, we find $\dot{R}_1 = 0$. However, the additional factor of x in the dust energy density proportional to $f(R)F'/R^2R'$ then shows that we can allow a quadratic term F_2x^2 in the mass function

to produce the desired regular expansion for energy density, although the total effective energy density is still diverging at the center because of the “vacuum” contributions in (104).

Using the various series expansions in (66), to lowest order in x we get

$$\dot{R}_1^2 = \frac{2^{3/2}e^{\frac{1}{2}-\frac{\pi}{4}}F_2}{(\gamma\ell_P^2)^{1/2}} \quad (114)$$

which is solved by

$$R_1(t) = 1 \pm \left[\frac{2^{3/2}e^{\frac{1}{2}-\frac{\pi}{4}}F_2}{(\gamma\ell_P^2)^{1/2}} \right]^{1/2} (t_0 - t) \quad (115)$$

where the plus sign corresponds to a collapsing dust cloud and where we have chosen the initial condition $R_1(t_0) = 1$. From here we see that the central singularity, corresponding to $R_1(t) = 0$ is formed at

$$t = t_0 + \left[\frac{2^{3/2}e^{\frac{1}{2}-\frac{\pi}{4}}F_2}{(\gamma\ell_P^2)^{1/2}} \right]^{-1} \quad (116)$$

For the sake of comparison we note that classically the central singularity forms at $t = t_0 + 2/3\sqrt{F_3}$. In terms of the initial density profile, $F_3 = 8\pi G\epsilon_0(0)/3$ (note that $\epsilon_0(0)$ is not the complete dust density profile at the initial time but a coefficient in the series expansion for the dust density) and therefore in terms of the initial density the time for singularity formation is $t = t_0 + 1/\sqrt{6\pi G\epsilon_0}$. For the quantum corrected case a similar consideration gives $F_2 = 4\pi G\epsilon_0(\gamma\ell_P^2)^{1/2}/2^{3/2}e^{\frac{1}{2}-\frac{\pi}{4}}$ which implies that the central singularity forms at $t = t_0 + 1/\sqrt{4\pi G\epsilon_0}$.

For the second version of inverse triad corrections, the equation to be solved is $\dot{R}^2 R = \alpha^2 F$ from (73). For small R , (113) implies that the lowest order term on the right hand side goes as x^9 if we use the same form of the expansion of $F(x)$ as classically. In this case, we can show $\dot{R}_1 = 0$ as in the first version. However, now our density is $\epsilon \propto (\alpha^2 F')/R^2 R'$ if the divergent “vacuum” contribution is subtracted, which means that $\alpha^2 F$ should be required to have a leading term cubic in x , such that F itself can have lower order terms. In this case, the singularity is not prevented either. Nevertheless, a finite neighborhood may look different from the classical space-time near a central singularity which, however, would require a more detailed analysis.

For our version of holonomy corrections, the equation to be solved is (92). After expanding in powers of x and equating the coefficients on the two sides we obtain (to order x^2) $R_1 \dot{R}_1^2 = F_3$ which is the same as in the classical case and gives

$$R_1(t) = \left(1 - \frac{3}{2}\sqrt{F_3}(t - t_0) \right)^{2/3} \quad (117)$$

implying that the singularity occurs at time $t = t_0 + 2/3\sqrt{F_3}$ (the same as in the classical case). At order x^3 we have the equation for R_2 which also does not have any quantum

corrections. Effects of the $\gamma^2\delta^2$ factor occur only at order x^4 and higher. Thus the small x behaviour with this correction is the same as for the classical LTB model. The combinations of inverse triad and holonomy corrections in (94) and (96) lead to the same conclusions.

We conclude that there is no indication that the corrections implemented here prevent the LTB singularity from forming. In particular, naked singularities as they appear in these models do not seem resolved automatically by a loop quantization. Whether they are indeed naked singularities in the presence of quantum effects requires further analysis of the effective space-time: the surroundings of the singularity may be sufficiently different from the classical naked case such that the singularity becomes spacelike. However, we have shown that a situation which gives rise to a naked singularity classically also gives rise to a singularity (of some form) under the quantum effects considered here. An analysis whether naked singularities remain naked may be of interest in the context of cosmic censorship, which we will come back to in the numerical analysis.

A correction not considered here is the effect of K_x -holonomies which are computationally more complicated and may be crucial in some regimes. In fact, taking the general form (21) of classical solutions indicates that $K_\varphi = \dot{R} = \sqrt{F/R}$ is subdominant to

$$K_x = \dot{R}' = \sqrt{F/R} \left(\frac{F'}{2F} - \frac{1}{2} \frac{\sqrt{x} - tF'/F}{R^{3/2}} \right)$$

near $x = 0$. This may present a chance for holonomy corrections to remove the singularity, after all. However, the size of holonomy corrections is also state-dependent: a small ℓ_0 suppresses K_x -corrections even if K_x is large. Thus, as already noted these corrections cannot result in generic avoidance of singularities. (Note that also in [76] only K_φ -corrections were included, although the conclusion was that the Schwarzschild singularity could be resolved in this way.) This clearly shows the non-trivial behavior of inhomogeneous situations compared to homogeneous ones.

5.2 Numerical analysis

Although some analytical results are available, the region of intermediate values for R not in the asymptotic regimes $R \ll \sqrt{\gamma}\ell_P$ or $R \gg \sqrt{\gamma}\ell_P$ is difficult to analyze. We thus complement the preceding analysis by numerical studies of inverse triad corrections.

For the first version, we transform the constraint equation with

$$K \equiv \dot{R}^2 - \frac{F}{R}, \tag{118}$$

to

$$K' = -\frac{1}{2R^2} \left[K + \left(K + \frac{F}{R} \right) (\alpha(R) - 1) \right] (R^2)' + (f - 1)F', \tag{119}$$

$$\dot{R} = \pm \sqrt{K + \frac{F}{R}}. \tag{120}$$

We spatially integrate the constraint equation at each time step and evolve R using (120). The constraint is always satisfied within 10^{-4} accuracy. The spatial integration is done using a fourth-order scheme while the time evolution uses a second-order scheme.

The second version is given by a set of equations which is first integrated by $R\dot{R}^2 = \alpha^2 F$. The numerical implementation of this equation is easy because we no longer need spatial integration. Our numerical scheme is second-order, which is sufficiently accurate and stable for the present purpose.

It should be noted that there is scale invariance in both sets of equations which are invariant under scaling $R(t, x)$, $F(x)$ and t as $R(t/\beta, x)$, $\beta^2 F(x)$ and t/β , where β is a positive constant. This scale invariance greatly simplifies the analysis. If the functional form of $F(x)$ is the same up to a constant factor, the evolution is similar up to the scaling of time. We thus do not need to investigate the full parameter space. Through this scaling, the classical Misner-Sharp mass m_{class} scales as $\beta^2 m_{\text{class}}$, while the corrected mass m does not. For holonomy corrections, the scaling behavior is lost. Here, a dedicated analysis of the whole parameter freedom is required to draw reliable conclusions, which we postpone to future work.

5.2.1 Initial condition

The function $F(x)$ corresponds to the conserved mass because it is constant for a comoving observer. Then,

$$\rho_{\text{cons}} \equiv \frac{F'}{8\pi G R^2 R'} \quad (121)$$

is regarded as the conserved mass density. Note that this differs from effective energy densities which incorporate quantum effects.

We choose the radial coordinate x so that

$$x = \frac{R_0(x)}{R_0(x_{\text{max}})}, \quad (122)$$

i.e. $0 \leq x \leq 1$ for the region of computation, where $R_0(x) \equiv R(0, x)$. As matter models, it is useful to consider two different cases: (i) uniform models where

$$F(x) = \begin{cases} F_0 x^3 & \text{for } 0 \leq x \leq x_s \\ F_1 & \text{for } x_s < x \end{cases} \quad (123)$$

and with

$$x_s = \frac{R_s}{R_0(x_{\text{max}})}, \quad F_0 = \frac{2GM}{x_s^3}, \quad F_1 = 2GM \quad (124)$$

in terms of the physical parameters given by the initial radius R_s and the total conserved mass M ; and (ii) quadratic models where

$$F(x) = \begin{cases} F_0 \left(\frac{x^3}{3} - \frac{x^5}{5x_s^2} \right) & \text{for } 0 \leq x \leq x_s \\ F_1 & \text{for } x_s < x \end{cases} \quad (125)$$

and

$$x_s = \frac{R_s}{R_0(x_{\max})} \quad , \quad F_0 = 15 \frac{GM}{x_s^3} \quad , \quad F_1 = 2GM . \quad (126)$$

Although we restrict ourselves to these two density profiles, there still are many possible sets of values for R_s and M . We choose $R_s = 1$ and 0.1 and $M = 0.01$, where the Planck length ℓ_P is chosen to be unity. In units used for the numerical analysis, we have a critical radius $R_* = \sqrt{\gamma/2}\ell_P \sim 0.25\ell_P$. So, $R_s = 1$ and 0.1 represent the cases where the initial size of the dust cloud is above and below the critical one, respectively. As we have already seen, we can recover the general mass scale by rescaling $F(x)$ and t as $\beta^2 F(x)$ and t/β . In other words, the dynamics of the dust cloud follows this scaling relation. However, it should be noted that as the corrected Misner-Sharp mass will not scale in such a simple way, the kinematics of null geodesics on the corrected spacetime will not follow this scaling. This means that the condition for horizon formation may depend on the mass scale, i.e. β . Due to our choice for the mass parameter $M = 0.01$, we can see the correction effect on the null expansions very clearly. The outer boundary of the calculated region is chosen to be $R_0(x_{\max}) = 2$. Our calculation region covers both the classical and effective regimes.

We have implemented a convergence test to the exact solution for time integration: For $\alpha = 1$ and $f = 1$, we have the marginally bound Lemaitre-Tolman-Bondi solution

$$R_{\text{ex}}(t, x) = \left(R(0, x)^{3/2} - \frac{3}{2} \sqrt{F(x)t} \right)^{2/3} . \quad (127)$$

Fig. 2 shows the residual of the numerical solution $R_{n,i}$ from the exact solution $R_{\text{ex}}(t, x)$

$$|R_{n,i} - R_{\text{ex}}(t_n, x_i)| \quad (128)$$

for $R_{0,i} = 10$ and $R_{\text{ex}}(0, x_i) = 10$, where n and i label the time step and the spatial grid point, respectively. The dust parameters are set to $M = 1$ and $R_s = 10$. One can see that as we decrease the time step Δt while fixing $\Delta x = 0.05$, the residual decreases as $(\Delta t)^2$.

In the following we fix $\Delta x = 10^{-4}$, where $x = 1$ corresponds to the outer boundary of the calculated region. We have confirmed that the numerical solution will not qualitatively change if we double Δx . The time step Δt is chosen so that the physical quantities on each grid point will change their values within 1% at each time step.

5.2.2 Classical collapse

Since there is no characteristic scale in classical theory, we have two independent scalings of $R(t, x)$, $F(x)$ and t to $\eta R(t/\beta, x)$, $\beta^2 \eta^3 F(x)$ and t/β , where β and η are constants. Hence, we can recover the results for general radius and mass parameters from a simulation done with only one set of parameters.

Fig. 3 shows the collapse of an initially homogeneous ball in classical general relativity. The total conserved mass M is set to be 0.01 and the initial radius of the cloud surface R_s is set to be 0.1 . Fig. 3 (a) shows the evolution of the density profile, where the conserved

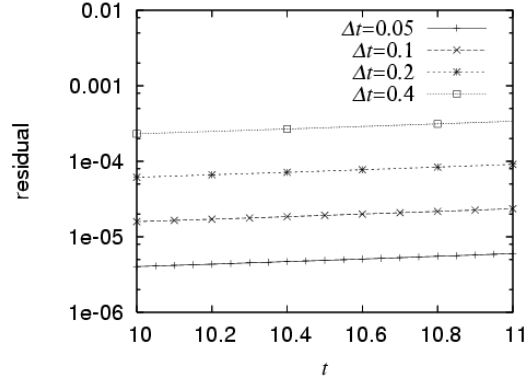


Figure 2: Convergence test for time integration.

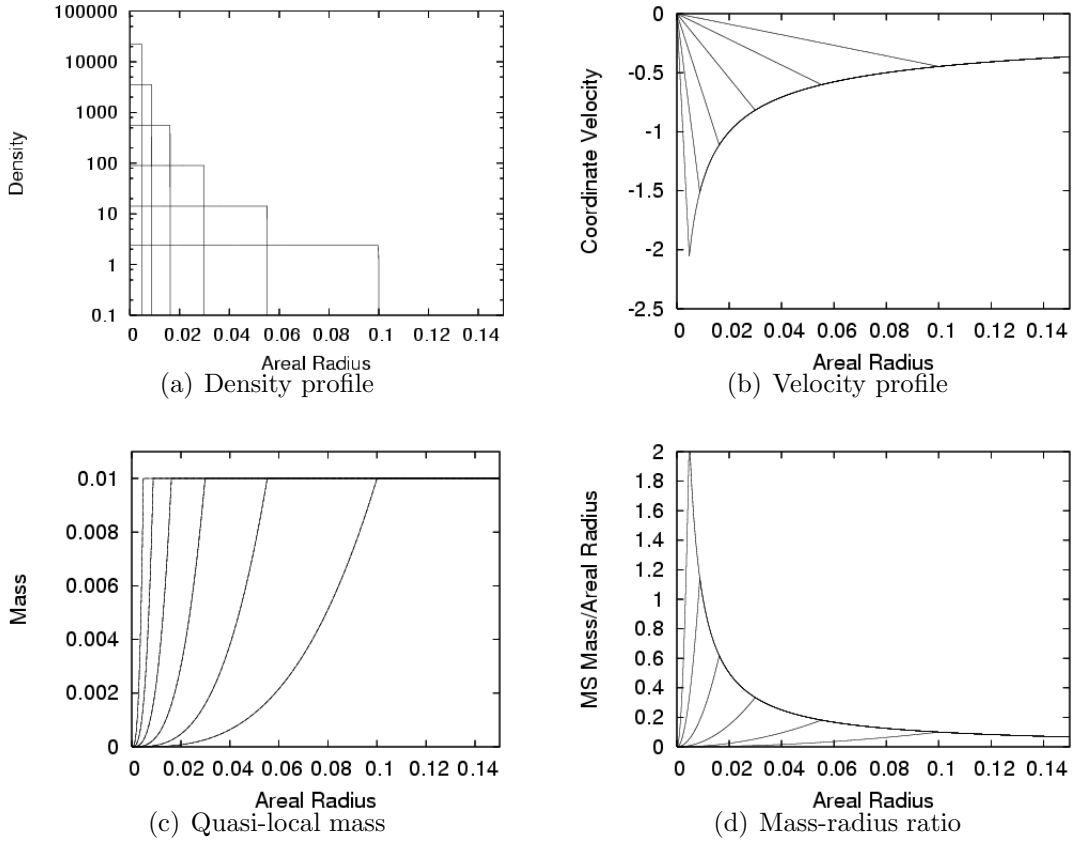


Figure 3: The collapse of a homogeneous dust ball with $R_s = 0.1$ and $M = 0.01$ in classical general relativity: the snapshots at $t = 0, 0.0887925729, 0.125072481, 0.139516828, 0.145267646$ and 0.147557255 are plotted.

mass density and the effective density coincide with each other in the classical case. Fig. 3 (b) shows the evolution of the velocity profile. Fig. 3 (c) shows the evolution of the mass profile, where also the conserved mass and the Misner-Sharp mass coincide with each other in this classical case. Fig. 3 (d) shows the evolution of the ratio between the Misner-Sharp mass m and the area radius R . This ratio becomes a half at trapping horizons. From Fig. 3 (a), we can see that the density profile in the ball remains uniform during the collapse. The solution is given by the marginally bound Oppenheimer-Snyder solution [98] where the singularity is massive and spacelike. In this exact solution, the singularity appears at $t = \sqrt{2}/3(0.1^3/0.01)^{1/2} \simeq 0.1490712\dots$. Not only an event horizon but also a trapping horizon always appear in this solution. The singularity is always hidden within the event horizon as well as the trapping horizon. Cosmic censorship holds in this collapse model.

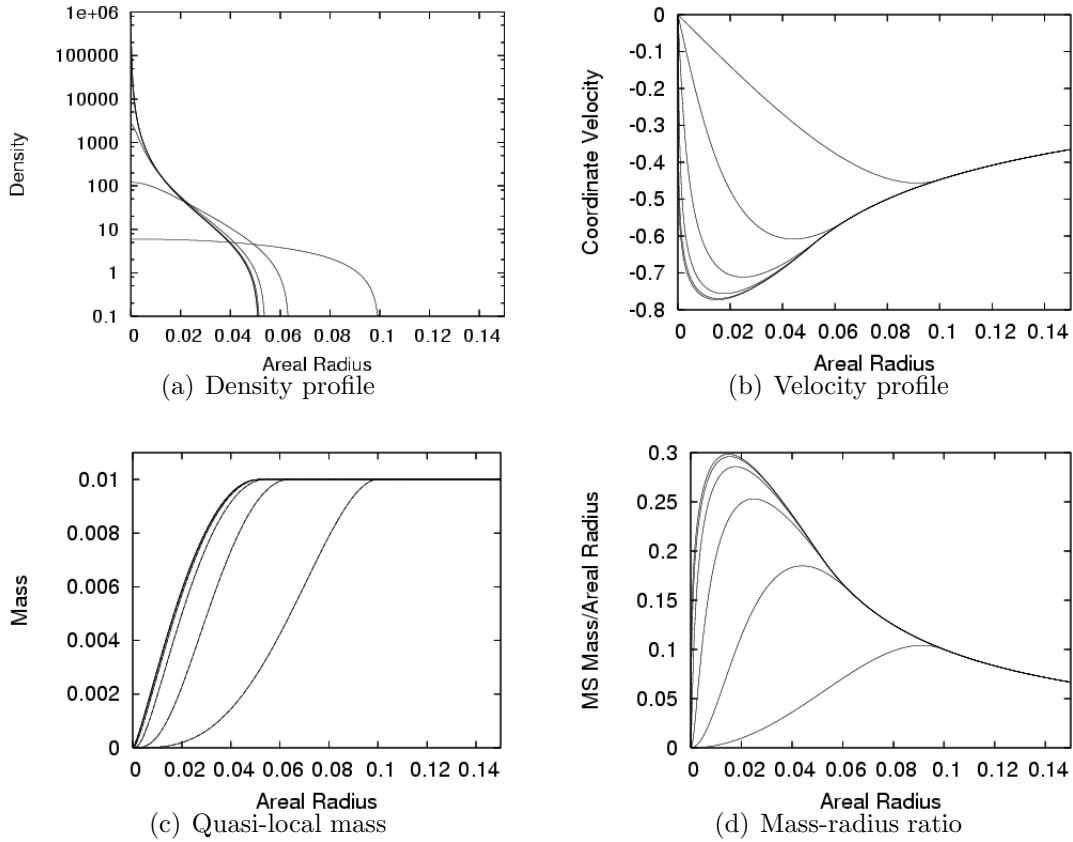


Figure 4: The collapse of an inhomogeneous dust ball with $R_s = 0.1$ and $M = 0.01$ in classical general relativity: the snapshots at $t = 0, 0.0736495616, 0.0898356836, 0.0933232155, 0.0940745701,$ and 0.0942363423 are plotted.

Fig. 4 shows the collapse of an initially inhomogeneous ball with $R_s = 0.1$ and $M = 0.01$ in classical general relativity. From Fig. 4 (a), we can see that the central density grows very rapidly while the surrounding region falls into the central region more slowly. This

induces strong inhomogeneity near the center and finally the calculation breaks down soon after $t = 0.0942363423$. In fact, the solution is exactly given by the marginally bound Lemaitre-Tolman-Bondi solution [21, 22, 23]. The peculiar behavior at the center seen in the numerical solution presents a shell-focusing singularity. In the present class of the Lemaitre-Tolman-Bondi solutions, the shell-focusing singularity has been shown to be massless, generic and locally naked [55], and moreover curvature strong [58, 59]. It can be globally naked depending on the values for R_s and M . We can determine whether a trapping horizon forms or not before the singularity formation by looking at the value of m/R shown in Fig. 4 (d), which gives a maximum of about 0.30 achieved at $t = 0.0942363423$. Although this might be slightly larger if we go closer to the singularity, the real value is not so different from 0.30. Since this ratio is a half at a trapping horizon, the present result means that no trapping horizon is formed in this case before the singularity is formed. The existence of a trapping horizon implies an event horizon outside or coinciding with it (but not vice versa) in classical general relativity [99].

5.2.3 Inverse triad corrections: First version

Fig. 5 shows the collapse of an initially homogeneous ball in the first version of consistent inverse triad corrections from loop quantum gravity with $R_s = 1$ and $M = 0.01$. Besides the conserved mass density ρ_{cons} , we can naturally define the effective density by

$$\rho_{\text{eff}} = \frac{m'}{4\pi GR^2 R'}. \quad (129)$$

This is defined so that when we integrate this with the invariant 3-dimensional volume element on the constant t spacelike hypersurface we recover the Misner-Sharp mass. This is directly related to the (t, t) -component of the Einstein curvature tensor and not necessarily positive definite.

Fig. 5 (a) shows the evolution of the profiles of both the conserved mass density (dashed line) and the effective density (solid line). We can see that the cloud becomes inhomogeneous in spite of its initial homogeneity. From Figs. 5 (a) and (b), we can see that the collapse is strongly slowed down in the central region $R \lesssim 0.05$, while the collapse continues to take place as in the classical case for the outer region $R \gtrsim 0.2$. As a result, as we can see in Fig. 5 (a), the conserved mass density at the central region remains almost unchanged, while it increases almost homogeneously in the outer region. We can also see in the same figure that the effective density is diverging at the center. As the cloud surface falls inside $R \simeq 0.2$, the effective density is still nonzero even outside the cloud surface. Moreover, for $0.11 \lesssim R \lesssim 0.24$ the effective density becomes negative, which is not shown in Fig. 5 (a). A spike develops also in the conserved mass density field at $R \simeq 0.06$ and then the calculation breaks down soon after $t = 4.56404342$. The spike in the conserved mass density field should be identified with a curvature singularity, which we can identify with the shell-crossing singularity as it also appears in the classical Lemaitre-Tolman-Bondi solution. Shell-crossing singularities can be naked but gravitationally weak [100, 101]. This singularity is so weak in curvature strength that it is generally believed to be extendible

in a distributional sense [52, 53]. Fig. 5 (c) shows the evolution of the Misner-Sharp mass and the conserved mass as a function of R . Although their total values are both 0.01, their distributions are quite different for $R \lesssim 1$. The Misner-Sharp mass dominates the conserved mass for $R \lesssim 0.2$. It takes a maximum $\simeq 0.04$ at $R \simeq 0.11$. The Misner-Sharp mass is a decreasing function of R for $0.11 \lesssim R \lesssim 0.24$, which implies the effective density is negative there. Fig. 5 (d) shows that the center is always marginally trapped. This is actually seen from the definition of the Misner-Sharp mass $m^{(I)}$ in Eq. (103). Except at the center the ratio m/R is less than a half, implying that the shell-crossing singularity is not covered by a trapping horizon.

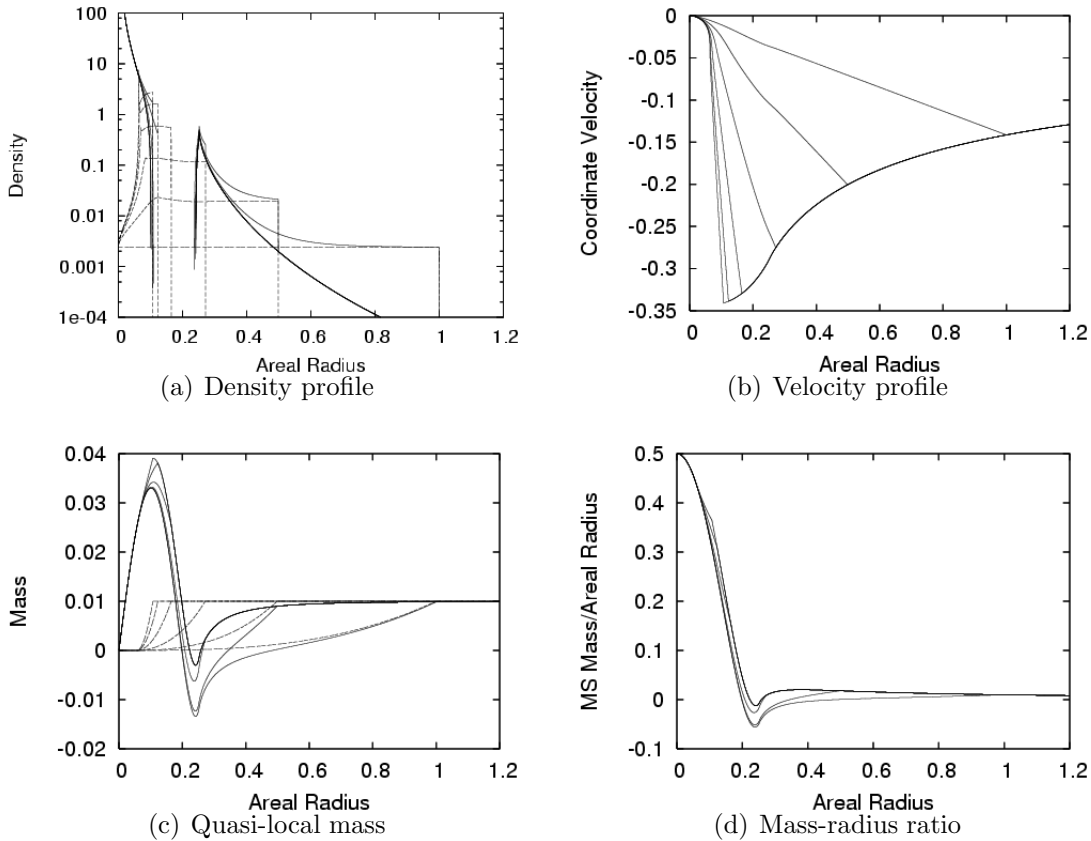


Figure 5: The collapse of a homogeneous dust ball with $R_s = 1$ and $M = 0.01$ in the first version of loop quantum gravity: the snapshots at $t = 0, 3.06904628, 4.04642236, 4.39347087, 4.51871685, \text{ and } 4.56404342$ are plotted. In (a), the solid and dashed lines denote the effective density and the conserved mass density, respectively. In (c), the solid and dashed lines denote the Misner-Sharp mass and the conserved mass, respectively.

Fig. 6 shows the collapse of an initially inhomogeneous ball with $R_s = 1$ and $M = 0.01$ in the first version of inverse triad corrections in loop quantum gravity. The qualitative properties are the same as in the initially uniform case. Also here, the collapse of the

central region $R \lesssim 0.05$ is strongly slowed down, while the outer dust falls onto the slowly collapsing central region. Again, a spike develops both in the effective density field and the conserved mass density field at $R \simeq 0.06$ and then the calculation breaks down soon after $t = 3.00299176$. The maximum value of m/R is a half attained at the center during this simulation as seen in Fig. 6(d). This means that for this case, no trapping horizon is formed before the spike or shell-crossing singularity is formed.

Without loop quantum effects, the collapse generically ends in the formation of a shell-focusing singularity. Hence, in regard of singularity formation, the collapse ends in a tamer shell-crossing singularity prior to the possible shell-focusing singularity due to the present loop quantum effects.

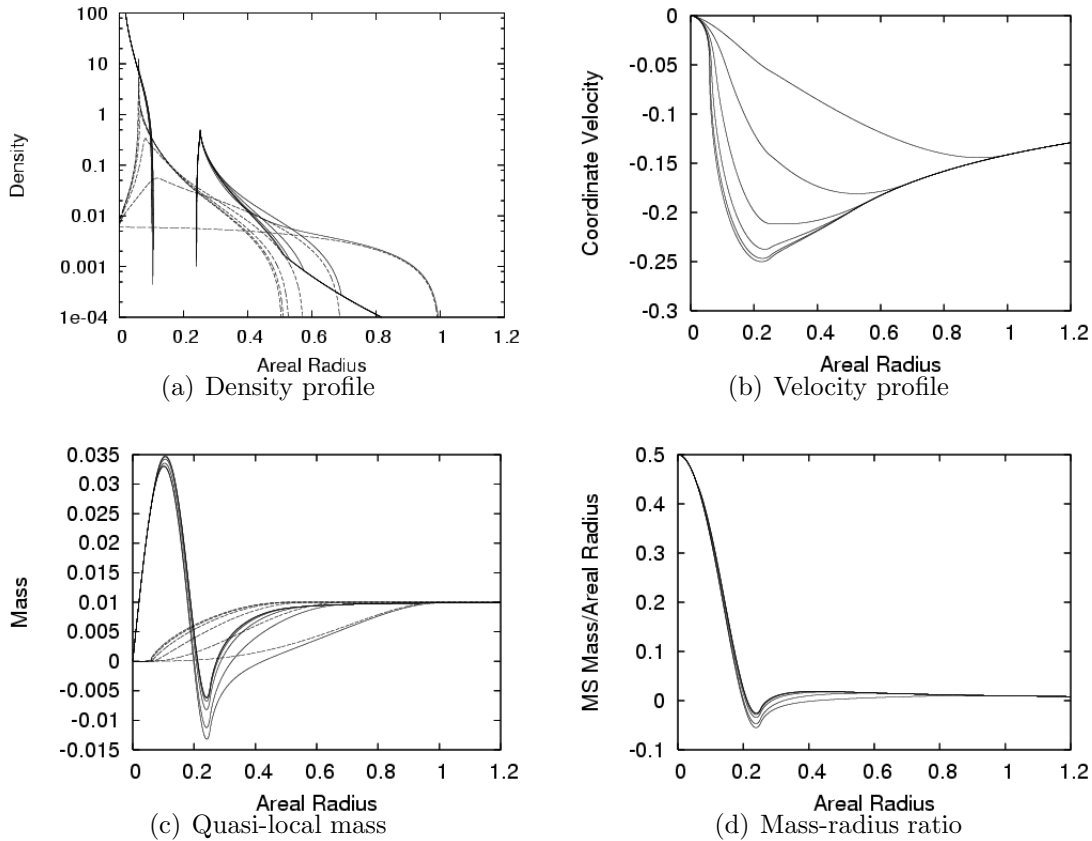


Figure 6: The collapse of an inhomogeneous dust ball with $R_s = 1$ and $M = 0.01$ in the first version of loop quantum gravity: the snapshots at $t = 0, 2.00754321, 2.65773896, 2.88917737, 2.97274431,$ and 3.00299176 are plotted. In (a), the solid and dashed lines denote the effective density and the conserved mass density, respectively. In (c), the solid and dashed lines denote the Misner-Sharp mass and the conserved mass, respectively.

If the initial radius of the cloud is smaller than the critical radius $R_* \simeq 0.25$, the situation becomes slightly different. Fig. 7 shows the collapse of a homogeneous dust ball

with $R_s = 0.1$ and $M = 0.01$. As seen in Fig. 7 (a), the conserved mass density has its maximum at the cloud surface. Then a spike develops at $R \simeq 0.046$ and the calculation breaks down soon after $t = 0.156702662$. The effective density outside the cloud is positive for $R \lesssim 0.11$ but negative for $0.11 \lesssim R \lesssim 0.24$. The Misner-Sharp mass takes its maximum value at $R \simeq 0.11$. Outside the cloud, the profile of the Misner-Sharp mass and therefore the effective density are almost unchanged compared to the classical behavior as seen in Fig. 7 (c). In fact, this feature is also seen for the cases where the initial radius is larger than the critical radius. Fig. 7 (d) shows that the maximum value of the ratio m/R greater than a half and this is attained at $R \simeq 0.046$, which implies that the shell-crossing singularity is covered by a trapping horizon in this case.

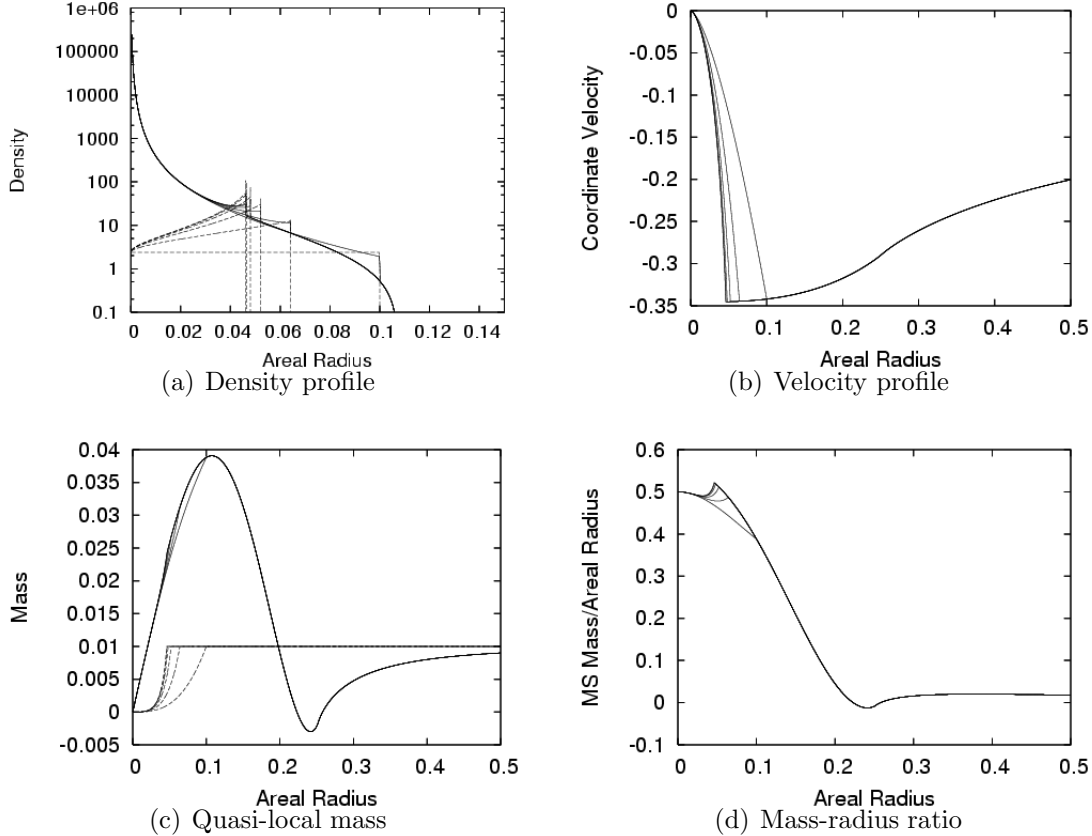


Figure 7: The collapse of a homogeneous dust ball with $R_s = 0.1$ and $M = 0.01$ in the first version of loop quantum gravity: the snapshots at $t = 0, 0.105124094, 0.139369943, 0.151074789, 0.155215854,$ and 0.156702662 are plotted. In (a), the solid and dashed lines denote the effective density and the conserved mass density, respectively. In (c), the solid and dashed lines denote the Misner-Sharp mass and the conserved mass, respectively.

For the collapse of an initially inhomogeneous ball, which is shown in Fig. 8, the qualitative feature is almost the same. However, the central region where the collapse is strongly

slowed down is much smaller than in the case where the initial radius is larger than the critical radius. As a result, a spike develops at the radius $R \simeq 0.012$. The shell-crossing singularity is covered by a trapping horizon in this case.

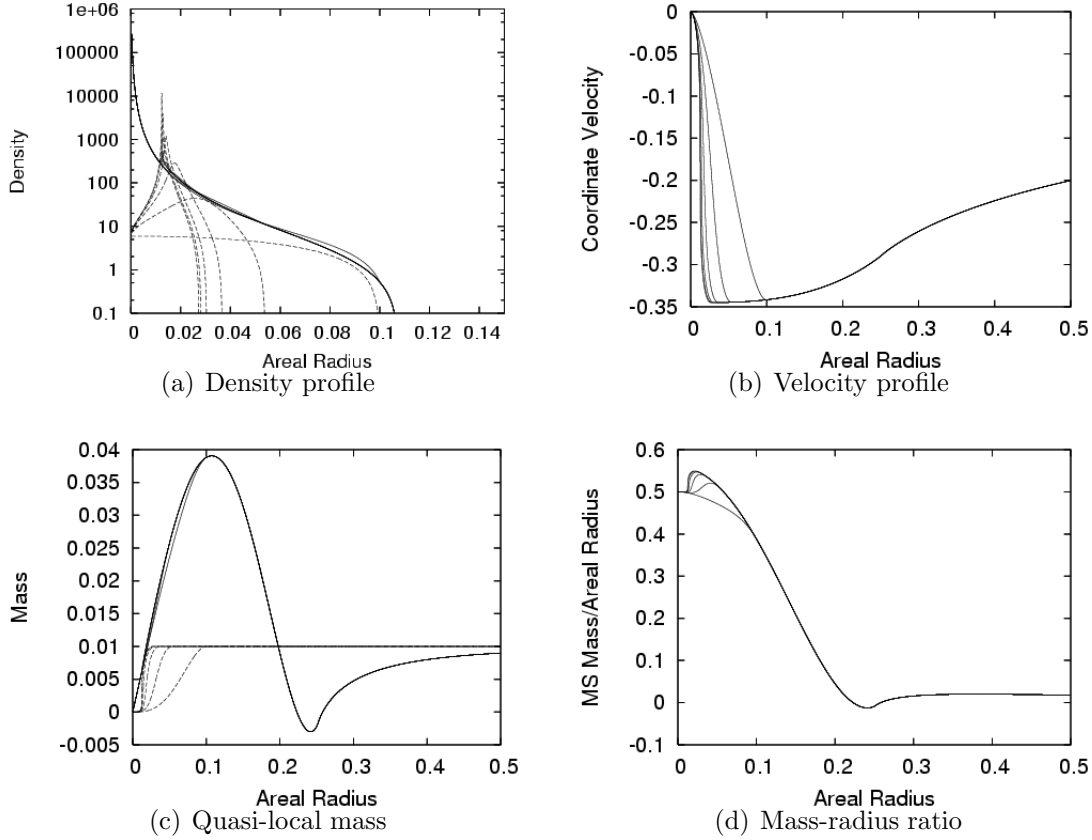


Figure 8: The collapse of an inhomogeneous dust ball $R_s = 0.1$ and $M = 0.01$ in the first version of loop quantum gravity: the snapshots at $t = 0, 0.134900072, 0.18447396, 0.202429874, 0.208934676, 0.211291203$ are plotted. In (a), the solid and dashed lines denote the effective density and the conserved mass density, respectively. In (c), the solid and dashed lines denote the Misner-Sharp mass and the conserved mass, respectively.

5.2.4 Inverse triad corrections: Second version

Fig. 9 shows the collapse of an initially homogeneous ball with $R_s = 1$ and $M = 0.01$ in the second version of consistent inverse triad corrections in loop quantum gravity. We can easily see that in spite of the very different formulation, the key feature that the collapse of the central region is strongly slowed down is the same as in the first version. The radius of this almost stopped central region is $\simeq 0.2$, which is much larger than in the first version.

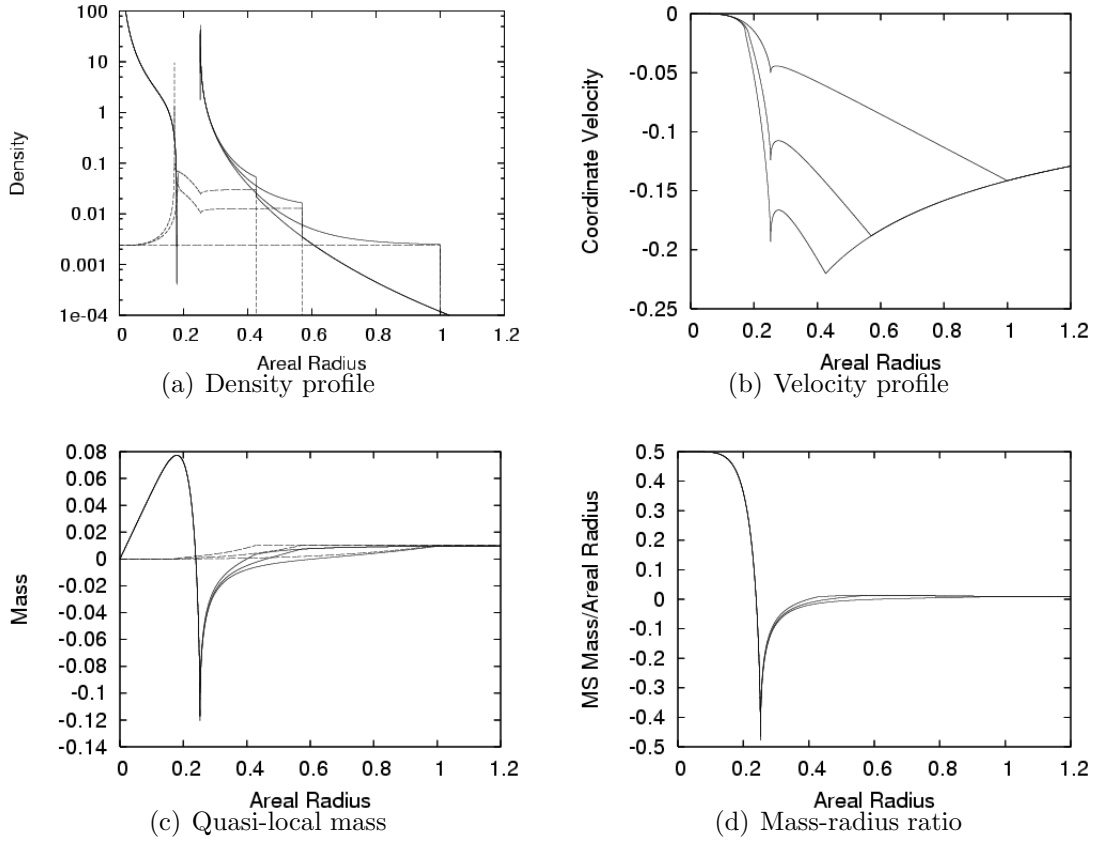


Figure 9: The collapse of a homogeneous dust ball with $R_s = 1$ and $M = 0.01$ in the second version of loop quantum gravity: the snapshots at $t = 0, 1.43300373, 2.34719999, 2.95414244, 3.36400543,$ and 3.39105418 are plotted. In (a), the solid and dashed lines denote the effective density and the conserved mass density, respectively. In (c), the solid and dashed lines denote the Misner-Sharp mass and the conserved mass, respectively.

In the conserved mass density profile a spike develops at $R \simeq 0.19$, $t = 3.39105418$. There is a dip in the profile of the conserved mass density at $R \simeq 0.25$, which corresponds to the critical radius $R = R_*$. For $R \gtrsim R_*$, the collapse proceeds as it does classically. As in the first version, the effective density is diverging at the center. If we go further outside, it decreases very rapidly to negative values and then turns to increase to positive values. The velocity profile shows two minimum values at the cloud surface and at $R \simeq R_*$ as seen in Fig. 9 (b). The Misner-Sharp mass dominates the conserved mass for $R \lesssim 0.2$ and it has a maximum about 0.08 at $R \simeq 0.18$ as seen in Fig. 9 (c). The center is always marginally trapped and the surrounding region is untrapped. Hence, the shell-crossing singularity is not covered by a trapping horizon.

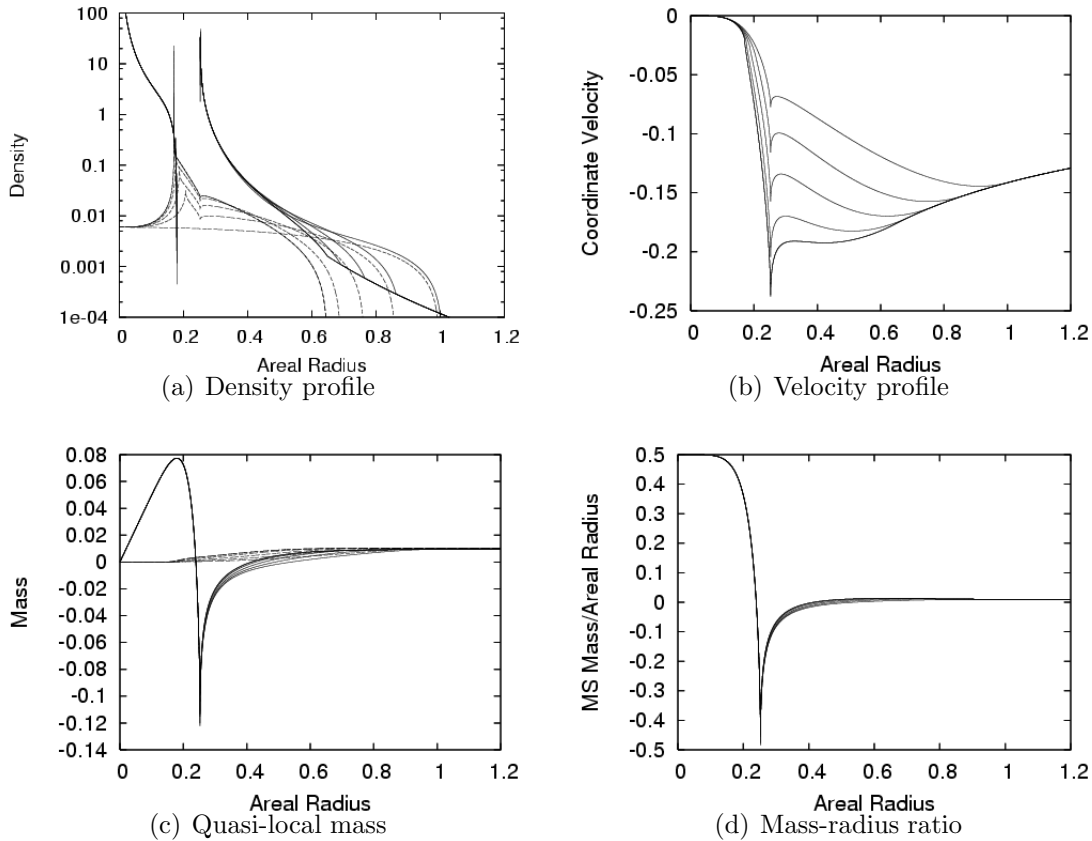


Figure 10: The collapse of an inhomogeneous dust ball with $R_s = 1$ and $M = 0.01$ in the second version of loop quantum gravity: the snapshots at $t = 0, 0.937882973, 1.5570413, 2.00350064, 2.2452289, \text{ and } 2.2463422$ are plotted. In (a), the solid and dashed lines denote the effective density and the conserved mass density, respectively. In (c), the solid and dashed lines denote the Misner-Sharp mass and the conserved mass, respectively.

Fig. 10 shows the evolution of an initially inhomogeneous dust ball with $R_s = 1$ and $M = 0.01$ in the second version of loop quantum gravity. The qualitative features are

common with the homogeneous case except that the velocity profile has only one minimum during the late stage of collapse. A spike develops in the density fields at $R \simeq 0.19$, $t = 2.2452289$. The spike or shell-crossing singularity is not covered by a trapping horizon.

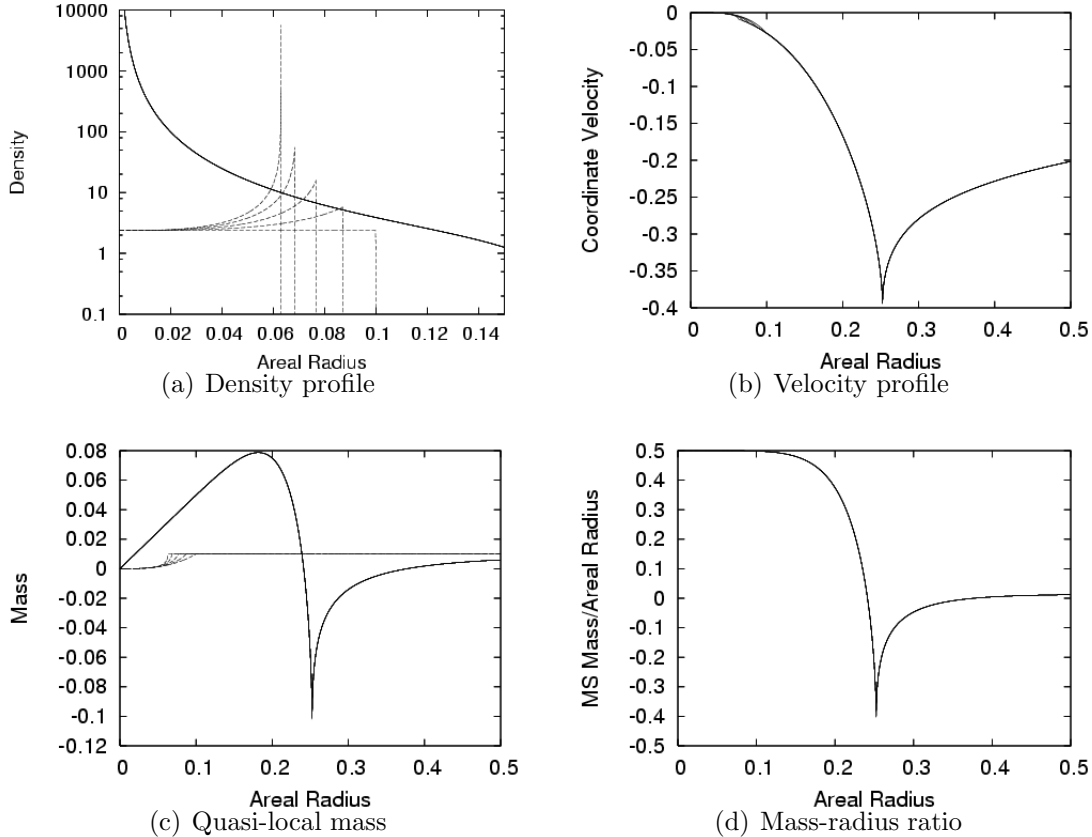


Figure 11: The collapse of a homogeneous dust ball with $R_s = 0.1$ and $M = 0.01$ in the second version formulation of loop quantum gravity: the snapshots at $t = 0, 0.550926063, 1.1729359, 1.83622205, \text{ and } 2.39522102$ are plotted. In (a), the solid and dashed lines denote the effective density and the conserved mass density, respectively. In (c), the solid and dashed lines denote the Misner-Sharp mass and the conserved mass, respectively.

Fig. 11 shows the evolution of an initially homogeneous dust ball with $R_s = 0.1$ and $M = 0.01$. In this case, the collapse proceeds very slowly in comparison to the classical evolution. It should be noted that in classical general relativity, the collapse ends in singularity formation at $t = \sqrt{2}/3 \times (0.1^3/0.01)^{1/2} \simeq 0.1490712 \dots$. In the second version of loop quantum gravity, the velocity field is kept very small within the whole cloud as seen in Fig. 11 (b). The profile of the conserved mass density shows a spike developing at the cloud surface at $R \simeq 0.062$ as seen in Fig. 11 (a). The simulation breaks down due to this spike soon after $t = 2.39522102$. The profile of the effective density is very different from that of the conserved mass density. The effective density becomes negative

for $0.18 \lesssim R \lesssim 0.25$. This is seen better in Fig. 11 (c). The maximum value of the Misner-Sharp mass is about 0.08. The maximum value of the ratio m/R is a half, which is attained at the center. Hence, the spike or shell-crossing singularity is not covered by a trapping horizon.

Finally, Fig. 12 shows the collapse of an initially inhomogeneous dust cloud with $R_s = 0.1$ and $M = 0.01$ in the second version of loop quantum gravity. Also in this case, the evolution is strongly slowed down. As seen in Fig. 12 a spike develops in the density fields inside the cloud at $R \simeq 0.04$, $t = 6.4440209$. The evolution outside the cloud is identical to that in the homogeneous case. The Misner-Sharp mass profile and therefore the effective density profile are almost constant in time. The maximum value of the Misner-Sharp mass is about 0.08 attained at $R \simeq 0.18$. The maximum value of the ratio m/R is a half attained at the center, which implies the spike or shell-crossing singularity is not covered by a trapping horizon.

5.3 Summary of the numerical analysis

In summary, the numerical results show that the loop quantum effects significantly slow down the collapse of the central region which is as large as $\sqrt{\gamma}l_P$, while in the outer region these effects are not important. (There are however quantitative differences between the different versions of consistent equations. In the second version the collapse of the central region is more strongly slowed down and the radius of this central “core” is larger than in the first version.) As a result, the density spike develops at around the radius $\sqrt{\gamma}l_P$, which results in the formation of a shell-crossing singularity. Another key feature is that the center is always marginally trapped due to the inverse triad correction to the metric. This suggests that the shell-focusing singularity appearing at the center might be covered by a horizon.

Since the collapse of an inhomogeneous dust cloud in classical general relativity generically ends in shell-focusing naked singularities, this means that although the singularity formed in the generic spherical dust collapse in the present formulation of loop quantum gravity is still locally naked, the shell-crossing singularity appears prior to the shell-focusing singularity and hence the curvature strength of locally naked singularities formed in the gravitational collapse is weakened due to the loop quantum effects. In a naive sense, this seems to favor the cosmic censorship hypothesis in effective loop quantum gravity because shell-crossing singularities are generally believed to be extendible in a distributional sense. Moreover, since the shell-crossing singularity will appear near the center, it is likely to be trapped due to the inverse triad correction to the metric. We have seen that this is the case for some collapse models in the first version.

However, one should be careful with any definite conclusion because the present work can only provide insights into some of the quantum effects in gravitational collapse and spacetime singularities. (For instance, as mentioned earlier we have not included holonomy effects in the numerical analysis because that would require a more detailed analysis of the parameter space.) The slow-down of the collapse indicates that repulsive forces of quantum gravity are indeed at work, similar to those that resolve big bang singularities in

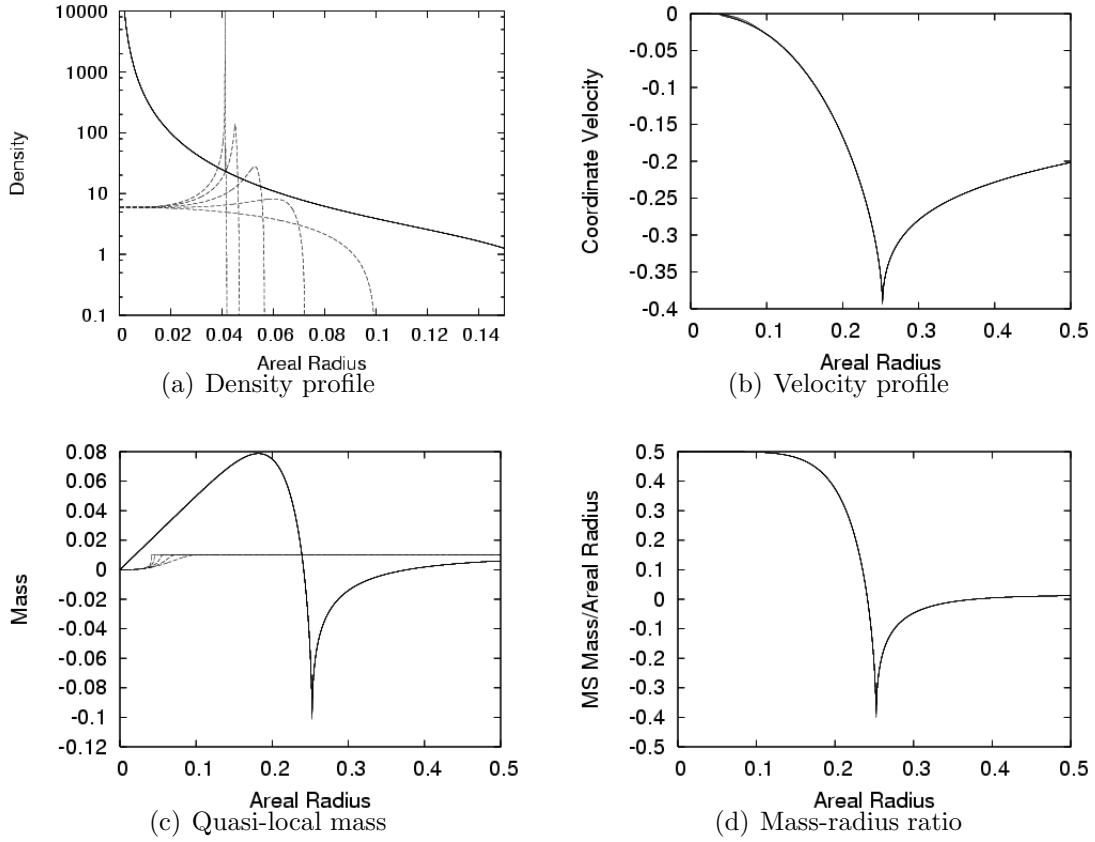


Figure 12: The collapse of an inhomogeneous dust ball with $R_s = 0.1$ and $M = 0.01$ in the second version formulation of loop quantum gravity: the snapshots at $t = 0, 1.50057314, 3.23870859, 5.12101428, 6.4440209$ are plotted. In (a), the solid and dashed lines denote the effective density and the conserved mass density, respectively. In (c), the solid and dashed lines denote the Misner-Sharp mass and the conserved mass, respectively.

homogeneous models. But in our inhomogeneous context this does not appear sufficient to provide a uniform bound on energy densities. The more complicated nature of the problem is indicated by the formation of shell-crossing singularities which may be a consequence of the still present spherical symmetry and the dust idealization used for matter.

6 Conclusions

We have analyzed the existence of LTB-type models in the framework of loop quantum gravity, starting with an implementation of the corresponding class of spatial metrics at the kinematical Hilbert space level. We first discussed the spherically symmetric setting and in particular noted the role of lattice refinements in Sec. 3.4. The discussion turned out to be much cleaner than in purely homogeneous settings, especially regarding the scale dependence of quantum equations. As an immediate consequence, not all refinement models used so far for anisotropic homogeneous models can be embedded in spherically symmetric models. In particular, non-trivial refinement schemes which would give rise to equidistant difference equations (where point holonomies are of the form $\exp(i\mu(p^I)c_I)$ with only the variable p^I conjugate to a connection component c_I entering) do not seem realizable in spherical symmetry. It is thus important to improve the analysis of non-equidistant difference equations, for instance along the lines of [102, 103]. Despite some restrictions on the refinement scheme, a whole class of refinements varying with the spatial size remains allowed. All these schemes have the correct scaling behavior under coordinate changes, even though further reduction to homogeneous models may suggest improper scalings for some of these models. This shows that it is only the reduction to homogeneity which may suggest improper scalings because scaling-dependent parameters arising in the reduction are overlooked. The restriction of refinement models based solely on their rescaling behavior in homogeneous models is thus too strict.

We then turned to the LTB conditions and showed that the classical conditions translate easily to the kinematical quantum level, which allows further studies of quantum reduction mechanisms of loop quantum gravity along the lines of [7]. However, the constraint algebra makes a discussion difficult at the dynamical level where the consistency issue of the operator algebra of constraints together with LTB conditions would have to be analyzed. At this stage, further progress is possible based on an effective treatment of correction terms. While we have not derived complete effective equations which would contain all relevant correction terms at once, the inclusion of individual correction terms of certain types can already be used to see how quantum effects can be realized consistently.

Indeed, we have found consistent formulations of the LTB reduction for different types of corrections: the constraint equations (66), (73) and (92) with the evolution equations (67), (74) and (91), respectively. Moreover, the effects can be combined in consistent equations summarized in Sec. 4.2. The consistency of an anomaly-free formulation relates corrections in different terms of the Hamiltonian to each other, but also to required corrections of the classical LTB conditions. Here, our general understanding of an LTB-type reduction is that metric coefficients in (2) are related to each other by a proportionality $L \propto R'$. Classically,

the factor is one, but consistent quantum corrections require a non-trivial dependence on R or \dot{R} which would be important in some regimes. Thus, while we have the same type of reduction of degrees of freedom, explicit dynamical implications for the metric may change. In particular, the relation between L and R affects, for instance, the position and behavior of horizons in addition to what a change in the dynamical behavior of R would imply. Also the behavior near classical singularities changes due to correction factors in the metric which may even diverge right at a classical singularity. A complete space-time analysis of the resulting effective metrics remains to be done.

The change in the form of the metric had unexpected implications: Further reductions which are possible classically, such as Friedmann–Robertson–Walker solutions, no longer exist, although on large scales there are approximate such solutions. This is quite unexpected and suggests that caution is necessary regarding the dynamical realization of homogeneous models. Moreover, in combination with corrections to the classical equations of motion, we have seen new terms in effective densities which can become negative even where mass densities remain positive. Also numerical simulations suggest that repulsive forces of quantum gravity are active on small scales. All this can affect the horizon behavior as well as singularities if negative energies and corresponding repulsive forces become strong enough. However, our analysis of central singularities, which may be spacelike or non-spacelike, did not reveal any indication that they would be prevented completely. While spherically symmetric loop quantum gravity is singularity-free at a fundamental level of difference equations [12] (see also [104, 105] for Gowdy models), the development of intuitive geometrical pictures requires non-singular equations for an effective geometry. We have not analyzed full effective equations and did not yet consider all possible correction terms; it may be that some of the corrections which are more complicated to include can avoid singularities more generally. Nevertheless, the difficulties in avoiding inhomogeneous singularities, in contrast to the fact that several spacelike singularities have been shown to be prevented based on homogeneous models of loop quantum gravity, suggest that general singularities present a qualitatively different issue compared to what has been realized so far. From our numerical simulations we might speculate a possible resolution mechanism more subtle than the analog of a cosmological bounce: Strong curvature singularities seem to be replaced by weak singularities which may be extendable by distributional solutions or with more realistic matter models.

Acknowledgements

We are grateful to T.P. Singh for several discussions and for valuable comments on the manuscript. M.B. thanks T.P. Singh for hospitality at TIFR, where some of this work was done. He was supported in part by NSF grant PHY0653127. T.H. thanks K. Nakao for helpful comment. He was supported by the Grant-in-Aid for Scientific Research Fund of the Ministry of Education, Culture, Sports, Science and Technology, Japan (Young Scientists (B) 18740144). R.T. thanks Ghanshyam Date for useful discussions and hospitality at IMSc, where some of this work was done.

References

- [1] T. Thiemann and H. A. Kastrup, Canonical Quantization of Spherically Symmetric Gravity in Ashtekar's Self-Dual Representation, *Nucl. Phys. B* 399 (1993) 211–258, [gr-qc/9310012]
- [2] H. A. Kastrup and T. Thiemann, Spherically Symmetric Gravity as a Completely Integrable System, *Nucl. Phys. B* 425 (1994) 665–686, [gr-qc/9401032]
- [3] K. V. Kuchař, Geometrodynamics of Schwarzschild Black Holes, *Phys. Rev. D* 50 (1994) 3961–3981
- [4] C. Rovelli, *Quantum Gravity*, Cambridge University Press, Cambridge, UK, 2004
- [5] A. Ashtekar and J. Lewandowski, Background independent quantum gravity: A status report, *Class. Quantum Grav.* 21 (2004) R53–R152, [gr-qc/0404018]
- [6] T. Thiemann, *Introduction to Modern Canonical Quantum General Relativity*, Cambridge University Press, Cambridge, UK, 2007, [gr-qc/0110034]
- [7] M. Bojowald and H. A. Kastrup, Symmetry Reduction for Quantized Diffeomorphism Invariant Theories of Connections, *Class. Quantum Grav.* 17 (2000) 3009–3043, [hep-th/9907042]
- [8] M. Bojowald, Spherically Symmetric Quantum Geometry: States and Basic Operators, *Class. Quantum Grav.* 21 (2004) 3733–3753, [gr-qc/0407017]
- [9] M. Bojowald and R. Swiderski, Spherically Symmetric Quantum Geometry: Hamiltonian Constraint, *Class. Quantum Grav.* 23 (2006) 2129–2154, [gr-qc/0511108]
- [10] M. Bojowald, *Quantum Riemannian Geometry and Black Holes*, Nova Science, 2006, [gr-qc/0602100]
- [11] M. Campiglia, R. Gambini, and J. Pullin, Loop quantization of spherically symmetric midi-superspaces, *Class. Quantum Grav.* 24 (2007) 3649, [gr-qc/0703135]
- [12] M. Bojowald, Non-singular black holes and degrees of freedom in quantum gravity, *Phys. Rev. Lett.* 95 (2005) 061301, [gr-qc/0506128]
- [13] M. Bojowald, Singularities and Quantum Gravity, *AIP Conf. Proc.* 910 (2007) 294–333, [gr-qc/0702144], Proceedings of the XIIth Brazilian School on Cosmology and Gravitation
- [14] P. S. Joshi, Gravitational Collapse: The Story so far, *Pramana* 55 (2000) 529
- [15] T. Harada, H. Iguchi, and K. Nakao, Physical Processes in Naked Singularity Formation, *Prog. Theor. Phys.* 107 (2002) 449–524

- [16] T. Harada, Gravitational Collapse and Naked Singularities, *Pramana* 63 (2004) 741–754
- [17] V. Husain and O. Winkler, Quantum resolution of black hole singularities, *Class. Quantum Grav.* 22 (2005) L127–L133, [gr-qc/0410125]
- [18] V. Husain and O. Winkler, Quantum black holes from null expansion operators, *Class. Quantum Grav.* 22 (2005) L135–L141, [gr-qc/0412039]
- [19] V. Husain and O. Winkler, Quantum Hamiltonian for gravitational collapse, *Phys. Rev. D* 73 (2006) 124007, [gr-qc/0601082]
- [20] J. Gegenberg, G. Kunstatter, and R. D. Small, Quantum Structure of Space Near a Black Hole Horizon, *Class. Quantum Grav.* 23 (2006) 6087–6100, [gr-qc/0606002]
- [21] G. Lemaitre, *Ann. Soc. Sci. Bruxelles I A* 53 (1933) 51
- [22] R. C. Tolman, Effect of inhomogeneity on cosmological models, *Proc. Nat. Acad. Sci.* 20 (1934) 169–176
- [23] H. Bondi, Spherically symmetrical models in general relativity, *Mon. Not. R. Astron. Soc.* 107 (1947) 410–425
- [24] J. Engle, Quantum field theory and its symmetry reduction, *Class. Quant. Grav.* 23 (2006) 2861–2893, [gr-qc/0511107]
- [25] T. Koslowski, Reduction of a Quantum Theory, [gr-qc/0612138]
- [26] T. Koslowski, A Cosmological Sector in Loop Quantum Gravity, [arXiv:0711.1098]
- [27] J. Engle, Relating loop quantum cosmology to loop quantum gravity: symmetric sectors and embeddings, *Class. Quantum Grav.* 24 (2007) 5777–5802, [gr-qc/0701132]
- [28] M. Bojowald, Loop quantum cosmology and inhomogeneities, *Gen. Rel. Grav.* 38 (2006) 1771–1795, [gr-qc/0609034]
- [29] M. Bojowald, The dark side of a patchwork universe, *Gen. Rel. Grav.* 40 (2008) 639–660, [arXiv:0705.4398]
- [30] M. Bojowald, Large scale effective theory for cosmological bounces, *Phys. Rev. D* 75 (2007) 081301(R), [gr-qc/0608100]
- [31] M. Bojowald, H. Hernández, and A. Skirzewski, Effective equations for isotropic quantum cosmology including matter, *Phys. Rev. D* 76 (2007) 063511, [arXiv:0706.1057]
- [32] M. Bojowald, Quantum nature of cosmological bounces, *Gen. Rel. Grav.* (2008) to appear, [arXiv:0801.4001]

- [33] M. Bojowald, How quantum is the big bang?, *Phys. Rev. Lett.* 100 (2008) 221301, [arXiv:0805.1192]
- [34] M. Bojowald and A. Skirzewski, Effective Equations of Motion for Quantum Systems, *Rev. Math. Phys.* 18 (2006) 713–745, [math-ph/0511043]
- [35] M. Bojowald and A. Skirzewski, Quantum Gravity and Higher Curvature Actions, *Int. J. Geom. Meth. Mod. Phys.* 4 (2007) 25–52, [hep-th/0606232], Proceedings of “Current Mathematical Topics in Gravitation and Cosmology” (42nd Karpacz Winter School of Theoretical Physics), Ed. Borowiec, A. and Francaviglia, M.
- [36] M. Bojowald, B. Sandhöfer, A. Skirzewski, and A. Tsobanjan, Effective constraints for quantum systems, [arXiv:0804.3365]
- [37] M. Bojowald, H. Hernández, M. Kagan, P. Singh, and A. Skirzewski, Formation and evolution of structure in loop cosmology, *Phys. Rev. Lett.* 98 (2007) 031301, [astro-ph/0611685]
- [38] M. Bojowald, H. Hernández, M. Kagan, P. Singh, and A. Skirzewski, Hamiltonian cosmological perturbation theory with loop quantum gravity corrections, *Phys. Rev. D* 74 (2006) 123512, [gr-qc/0609057]
- [39] D. J. Mulryne and N. J. Nunes, Constraints on a scale invariant power spectrum from superinflation in LQC, *Phys. Rev. D* 74 (2006) 083507, [astro-ph/0607037]
- [40] G. Calcagni and M. V. Cortês, Inflationary scalar spectrum in loop quantum cosmology, *Class. Quantum Grav.* 24 (2007) 829–853, [gr-qc/0607059]
- [41] E. J. Copeland, D. J. Mulryne, N. J. Nunes, and M. Shaeri, Super-inflation in Loop Quantum Cosmology, [arXiv:0708.1261]
- [42] M. Bojowald and G. Hossain, Cosmological vector modes and quantum gravity effects, *Class. Quantum Grav.* 24 (2007) 4801–4816, [arXiv:0709.0872]
- [43] J. Mielczarek and M. Szydlowski, Relic gravitons as the observable for Loop Quantum Cosmology, *Phys. Lett. B* 657 (2007) 20–26, [arXiv:0705.4449]
- [44] M. Bojowald and G. Hossain, Quantum gravity corrections to gravitational wave dispersion, *Phys. Rev. D* 77 (2008) 023508, [arXiv:0709.2365]
- [45] M. Bojowald, Loop Quantum Cosmology, *Living Rev. Relativity* 8 (2005) 11, [gr-qc/0601085], <http://relativity.livingreviews.org/Articles/lrr-2005-11/>
- [46] S. A. Hayward, General laws of black-hole dynamics, *Phys. Rev. D* 49 (1994) 6467–6474

- [47] T. A. Roman and P. G. Bergmann, Stellar collapse without singularities?, *Phys. Rev. D* 28 (1983) 1265–1277
- [48] B. Krishnan and E. Schnetter, Non-symmetric trapped surfaces in the Schwarzschild and Vaidya spacetimes, *Phys. Rev. D* 73 (2006) 021502(R), [gr-qc/0511017]
- [49] I. Ben-Dov, Outer Trapped Surfaces in Vaidya Spacetimes, *Phys. Rev. D* 75 (2007) 064007, [gr-qc/0611057]
- [50] S. Barve, T. P. Singh, C. Vaz, and L. Witten, Particle creation in the marginally bound, selfsimilar collapse of inhomogeneous dust, *Nucl. Phys. B* 532 (1998) 361–375, [gr-qc/9802035]
- [51] G. Rein, A. D. Rendall, and J. Schaeffer, A regularity theorem for solutions of the spherically symmetric Vlasov-Einstein system, *Commun. Math. Phys.* 168 467–478
- [52] C. J. S. Clarke, *The Analysis of Space-Time Singularities*, Cambridge University Press, Cambridge, UK, 1993
- [53] B. C. Nolan, Dynamical extensions for shell-crossing singularities, *Class. Quantum Grav.* 20 (2003) 575–585, [gr-qc/0301028]
- [54] D. M. Eardley and L. Smarr, Time functions in numerical relativity: Marginally bound dust collapse, *Phys. Rev. D* 19 (1979) 2239–2259
- [55] D. Christodoulou, Violation of cosmic censorship in the gravitational collapse of a dust cloud, *Commun. Math. Phys.* 93 (1984) 171–195
- [56] T. P. Singh and P. S. Joshi, The final fate of spherical inhomogeneous dust collapse, *Class. Quantum Grav.* 13 (1996) 559–571, [gr-qc/9409062]
- [57] S. Jhingan and P. S. Joshi, The Structure of singularity in spherical inhomogeneous dust collapse, *Ann. Israel Phys. Soc.* 13 (1997) 357, [gr-qc/9701016]
- [58] R. P. A. C. Newman, Strengths of naked singularities in Tolman-Bondi spacetimes, *Class. Quantum Grav.* 3 (1986) 527–539
- [59] S. S. Deshingkar, P. S. Joshi, and I. H. Dwivedi, The Nature of central singularity in spherical dust collapse, *Phys. Rev. D* 59 (1999) 044018
- [60] C. Vaz and L. Witten, Mass Quantization of the Schwarzschild Black Hole, *Phys. Rev. D* 60 (1999) 024009, [arXiv:gr-qc/9811062]
- [61] C. Vaz, L. Witten, and T. P. Singh, Toward a Midisuperspace Quantization of LeMaitre-Tolman-Bondi Collapse Models, *Phys. Rev. D* 63 (2001) 104020, [arXiv:gr-qc/0012053]

- [62] C. Kiefer, J. Müller-Hill, and C. Vaz, Classical and quantum LTB model for the non-marginal case, *Phys. Rev. D* 73 (2006) 044025, [gr-qc/0512047]
- [63] R. Tibrewala, S. Gutti, T. P. Singh, and C. Vaz, Classical and Quantum Gravitational Collapse in d-dim AdS Spacetime I. Classical Solutions, *Phys. Rev. D* 77 (2008) 064012, [arXiv:0712.1413]
- [64] C. Vaz, R. Tibrewala, and T. P. Singh, Classical and Quantum Gravitational Collapse in d-dim AdS Spacetime II. Quantum States and Hawking Radiation, [arXiv:0805.0519]
- [65] J. F. Barbero G., Real Ashtekar Variables for Lorentzian Signature Space-Times, *Phys. Rev. D* 51 (1995) 5507–5510, [gr-qc/9410014]
- [66] G. Immirzi, Real and Complex Connections for Canonical Gravity, *Class. Quantum Grav.* 14 (1997) L177–L181
- [67] C. Kiefer, J. Müller-Hill, T. P. Singh, and C. Vaz, Hawking radiation from the quantum Lemaitre-Tolman-Bondi model, *Phys. Rev. D* 75 (2007) 124010, [gr-qc/0703008]
- [68] C. Vaz, S. Gutti, C. Kiefer, and T. P. Singh, Quantum Gravitational Collapse and Hawking Radiation in 2+1 Dimensions, *Phys. Rev. D* 76 (2007) 124021, [arXiv:0710.2164]
- [69] C. Rovelli and L. Smolin, Loop Space Representation of Quantum General Relativity, *Nucl. Phys. B* 331 (1990) 80–152
- [70] G. M. Hossain, Primordial Density Perturbation in Effective Loop Quantum Cosmology, *Class. Quantum Grav.* 22 (2005) 2511–2532, [gr-qc/0411012]
- [71] W. Nelson and M. Sakellariadou, Lattice Refining Loop Quantum Cosmology and Inflation, *Phys. Rev. D* 76 (2007) 044015, [arXiv:0706.0179]
- [72] W. Nelson and M. Sakellariadou, Lattice Refining LQC and the Matter Hamiltonian, *Phys. Rev. D* 76 (2007) 104003, [arXiv:0707.0588]
- [73] A. Barrau and J. Grain, Holonomy corrections to the cosmological primordial tensor power spectrum, Proceedings of the 43rd Rencontres de Moriond “Cosmology 2008,” [arXiv:0805.0356]
- [74] R. Gambini and J. Pullin, Canonical quantization of general relativity in discrete space-times, *Phys. Rev. Lett.* 90 (2003) 021301, [gr-qc/0206055]
- [75] M. Campiglia, C. Di Bartolo, R. Gambini, and J. Pullin, Uniform discretizations: a new approach for the quantization of totally constrained systems, *Phys. Rev. D* 74 (2006) 124012, [gr-qc/0610023]

- [76] R. Gambini and J. Pullin, Black holes in loop quantum gravity: the complete spacetime, [arXiv:0805.1187]
- [77] T. Thiemann, Quantum Spin Dynamics (QSD), *Class. Quantum Grav.* 15 (1998) 839–873, [gr-qc/9606089]
- [78] M. Bojowald, Inverse Scale Factor in Isotropic Quantum Geometry, *Phys. Rev. D* 64 (2001) 084018, [gr-qc/0105067]
- [79] J. Brunnemann and T. Thiemann, Unboundedness of Triad-Like Operators in Loop Quantum Gravity, *Class. Quantum Grav.* 23 (2006) 1429–1483, [gr-qc/0505033]
- [80] M. Bojowald, Degenerate Configurations, Singularities and the Non-Abelian Nature of Loop Quantum Gravity, *Class. Quantum Grav.* 23 (2006) 987–1008, [gr-qc/0508118]
- [81] T. Thiemann, QSD V: Quantum Gravity as the Natural Regulator of Matter Quantum Field Theories, *Class. Quantum Grav.* 15 (1998) 1281–1314, [gr-qc/9705019]
- [82] M. Bojowald, D. Cartin, and G. Khanna, Lattice refining loop quantum cosmology, anisotropic models and stability, *Phys. Rev. D* 76 (2007) 064018, [arXiv:0704.1137]
- [83] M. Bojowald, Quantization ambiguities in isotropic quantum geometry, *Class. Quantum Grav.* 19 (2002) 5113–5130, [gr-qc/0206053]
- [84] M. Bojowald, H. Hernández, M. Kagan, and A. Skirzewski, Effective constraints of loop quantum gravity, *Phys. Rev. D* 75 (2007) 064022, [gr-qc/0611112]
- [85] C. B. Böhrer and K. Vandersloot, Loop Quantum Dynamics of the Schwarzschild Interior, *Phys. Rev. D* 76 (2007) 104030, [arXiv:0709.2129]
- [86] D.-W. Chiou, Phenomenological dynamics of loop quantum cosmology in Kantowski-Sachs spacetime, [arXiv:0803.3659]
- [87] M. Bojowald, R. Goswami, R. Maartens, and P. Singh, A black hole mass threshold from non-singular quantum gravitational collapse, *Phys. Rev. Lett.* 95 (2005) 091302, [gr-qc/0503041]
- [88] H. Kudoh, T. Harada, and H. Iguchi, Birth of timelike naked singularity, *Phys. Rev. D* 62 (2000) 104016, [gr-qc/0006089]
- [89] G. T. Horowitz and R. C. Myers, The Value of Singularities, *Gen. Rel. Grav.* 27 (1995) 915–919, [gr-qc/9503062]
- [90] M. Bojowald, R. Maartens, and P. Singh, Loop Quantum Gravity and the Cyclic Universe, *Phys. Rev. D* 70 (2004) 083517, [hep-th/0407115]

- [91] P. Singh and A. Toporensky, Big Crunch Avoidance in $k = 1$ Semi-Classical Loop Quantum Cosmology, *Phys. Rev. D* 69 (2004) 104008, [gr-qc/0312110]
- [92] G. Date and G. M. Hossain, Genericity of Big Bounce in isotropic loop quantum cosmology, *Phys. Rev. Lett.* 94 (2005) 011302, [gr-qc/0407074]
- [93] A. Ashtekar, T. Pawłowski, and P. Singh, Quantum Nature of the Big Bang, *Phys. Rev. Lett.* 96 (2006) 141301, [gr-qc/0602086]
- [94] T. Tanaka and T. P. Singh, Analytic derivation of the map of null rays passing near a naked singularity, *Phys. Rev. D* 63 (2001) 124021, [gr-qc/0010110]
- [95] G. I. Barenblatt, *Scaling, Self-Similarity, and Intermediate Asymptotics*, Cambridge University Press, Cambridge, UK, 1996
- [96] A. A. Coley, Kinematic self-similarity, *Class. Quantum Grav.* 14 (1997) 87–118, [gr-qc/9610061]
- [97] H. Maeda and T. Harada, Kinematic self-similar solutions in general relativity, In: *General Relativity Research Trends*, Nova Science Publishers, New York, USA, 2005, Horizons in World Physics, Volume 249
- [98] J. R. Oppenheimer and H. Snyder, On Continued Gravitational Contraction, *Phys. Rev.* 56 (1939) 455–459
- [99] S. W. Hawking and G. F. R. Ellis, *The Large Scale Structure of Space-Time*, Cambridge University Press, 1973
- [100] P. Yodzis, H.-J. Seifert, and H. Müller zum Hagen, On the occurrence of naked singularities in general relativity, *Commun. Math. Phys.* 34 (1973) 135–148
- [101] H. Müller zum Hagen, P. Yodzis, and H.-J. Seifert, On the occurrence of naked singularities in general relativity. II, *Commun. Math. Phys.* 37 (1974) 29–40
- [102] S. Sabharwal and G. Khanna, Numerical solutions to lattice-refined models in loop quantum cosmology, *Class. Quantum Grav.* 25 (2008) 085009, [arXiv:0711.2086]
- [103] W. Nelson and M. Sakellariadou, Numerical techniques for solving the quantum constraint equation of generic lattice-refined models in loop quantum cosmology, [arXiv:0803.4483]
- [104] K. Banerjee and G. Date, Loop Quantization of Polarized Gowdy Model on T^3 : Quantum Theory, [arXiv:0712.0687]
- [105] M. Martín-Benito, L. J. Garay, and G. A. Mena Marugán, Hybrid Quantum Gowdy Cosmology: Combining Loop and Fock Quantizations, [arXiv:0804.1098]